DOI: 10.1016/j.cviu.2019.07.007

Computer Vision and Image Understanding
journal homepage: www.elsevier.com

Non-ideal iris segmentation using Polar Spline RANSAC and illumination compensation

Ruggero Donida Labati[a,**], Enrique Muñoz[a], Vincenzo Piuri[a], Arun Ross[b], Fabio Scotti[a]

[a] *Department of Computer Science, Università degli Studi di Milano, via Bramante, 65, I-26013 Crema (CR), Italy*
[b] *Department of Computer Science and Engineering, Michigan State University, 48824 East Lansing, MI, USA*

ABSTRACT

In this work, we propose a robust iris segmentation method for non-ideal ocular images, referred to as Polar Spline RANSAC, which approximates the iris shape as a closed curve with arbitrary degrees of freedom. The method is robust to several nonidealities, such as poor contrast, occlusions, gaze deviations, pupil dilation, motion blur, poor focus, frame interlacing, differences in image resolution, specular reflections, and shadows. Unlike most techniques in the literature, the proposed method obtains good performance in harsh conditions with different imaging wavelengths and datasets. We also investigate the role of different illumination compensation techniques on the iris segmentation process. The experiments showed that the proposed method results in higher or comparable accuracy with respect to other competing techniques presented in the literature for images acquired in non-ideal conditions. Furthermore, the proposed segmentation method is generalizable and can achieve competitive performance with different state-of-the-art feature extraction and matching techniques. In particular, in conjunction with a well-known recognition schema, it achieved Equal Error Rate of 4.34% on DB WVU, Equal Error Rate of 5.98% on DB QFIRE, and pixel-wise classification error rate of 0.0165 on DB UBIRIS v2. Moreover, experiments using different illumination compensation techniques demonstrate that algorithms based on the Retinex model offer improved segmentation and recognition accuracy, thereby highlighting the importance of adopting illumination models for processing non-ideal ocular images.

1. Introduction

Iris recognition refers to the automated process of recognizing individuals based on their iris pattern, Daugman (2002). Due to its distinctive texture that varies in its details across individuals, the iris is a powerful biometric trait and the recognition systems based on iris have been deployed in a wide range of applications such as national ID cards, border control, user authentication in smartphones, etc. Iris recognition systems perform accurately when iris images are acquired from cooperative users under reasonably controlled conditions since the accuracy of such systems can be negatively impacted by non-ideal conditions characterized by harsh illumination, non-cooperative or moving subjects and unconstrained acquisition. Designing methods to process such non-ideal images can significantly reduce the level of user cooperation necessary during the acquisition process, relax the acquisition constraints, and expand the possible applications for iris recognition systems.

One of the most challenging tasks in iris recognition is the segmentation of the iris region from the input ocular or face image. Segmentation algorithms must cope with the fact that the iris region is a relatively small area that is behind the moist cornea, constantly in motion, and frequently occluded by eyelids and eyelashes. Moreover, the quality of iris samples can be reduced by external factors, such as sensor noise, low cooperation from the user, poor illumination conditions, and large standoff distances (See Table 1). The resulting nonidealities manifest themselves in images acquired using traditional iris scanners or in images captured at a distance using digital cameras. Fig. 1 shows examples of non-ideal samples acquired using a commercial sensor (Irispass), Fig. 2 shows non-ideal im-

**Corresponding author: Tel.: +39-02-503-16377;
e-mail: ruggero.donida@unimi.it (Ruggero Donida Labati)

Table 1. Factors resulting in non-ideal iris images.

Source of nonideality	Effects
Acquisition sensor	Low signal-to-noise ratio (SNR) Frame interlacing Poor focus Motion blur
Low cooperation from the user	Strong occlusion Gaze deviation
Uncontrolled distance from the camera	Strong differences in iris radii Differences in illumination conditions
Illumination conditions	Low illumination High illumination and pixel saturation Non-constant illumination Pupil dilation Specular reflections Shadows

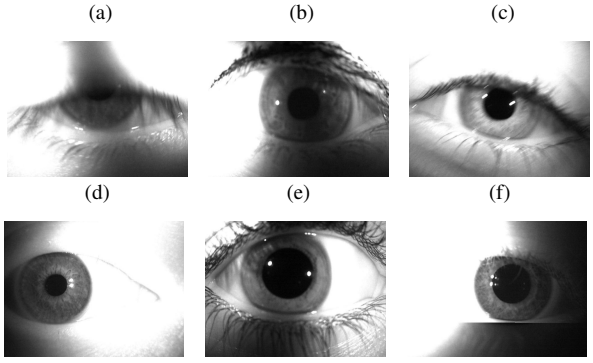

Fig. 1. Examples of nonidealities in iris images acquired using a commercial sensor (WVU database): (a) strong occlusion, (b) poor illumination, (c) blur due to poor focus or motion, (d) gaze deviation, (e) pupil dilation, and (f) interlacing. All the images have size of 640×480 pixels.

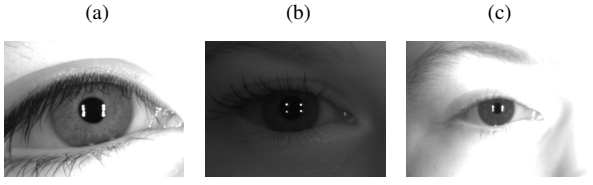

Fig. 2. Examples of non-ideal images acquired at different distances and illumination conditions using an infrared camera (Q-FIRE database): (a) medium illumination and large iris diameter, (b) low illumination and medium iris diameter, and (c) high illumination and small iris diameter. All the images shown have been obtained by cropping a frame with size 640×480 pixels centered in the virtual center of the pupil. The samples present strong differences in terms of iris diameter (from approximately 110 pixels to more than 300 pixels).

ages captured using an infrared camera (Dalsa 4M30) placed at varying distances from the subject (ranging from 5 to 25 feet), and Fig. 3 shows non-ideal images acquired in natural light and uncooperative conditions using a single-lens reflex digital camera (Canon 5D) placed at varying distances from the subject (ranging from 4 to 8 meters).

Different studies report that strong nonidealities in iris images (especially strong occlusions and poor illumination conditions) can severely impact the recognition accuracy of iris recognition systems, as Proenca and Alexandre (2012a); Jillela et al. (2013); Donida Labati et al. (2012); Schmid et al. (2013); Tabassi et al. (2011).

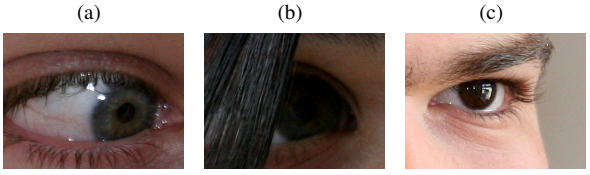

Fig. 3. Examples of non-ideal images acquired using a digital single-lens reflex digital camera in an uncooperative scenario, at different distances from the camera, and in natural light conditions (UBIRIS v.2 database): (a) gaze deviation, (b) occlusions, and (c) small iris diameter. All the images have size of 400×300 pixels.

Robust segmentation methods able to deal with non-ideal iris images acquired under poor illumination conditions should reliably extract the iris boundaries, i.e., the inner pupillary boundary and the outer limbus boundary, even if there are local regions that are underexposed or overexposed (see Fig. 1, Fig. 2, and Fig. 3).

To achieve this goal, this paper focuses on the design of an iris segmentation algorithm for non-ideal iris images acquired under poor illumination conditions and capable of working in different spectral bands. The algorithm can process ocular images acquired using both infrared and visible light illumination techniques. The first step of the method reduces the effect of specular reflections and noise. The second step is to estimate the internal iris boundary using an iterative algorithm. The third step is the illumination compensation. The final step is the segmentation of the external iris boundary using a novel method based on RANdom SAmple Consensus (RANSAC), which we refer to as Polar Spline RANSAC (PS-RANSAC). For the integration of this segmentation method into a complete iris biometric system, we also propose an iris normalization strategy in which the limits of the iris region are estimated from a segmentation mask. Fig. 4 shows the schema of the segmentation and template computation tasks of the iris recognition process.

The most important contribution of this work lies in the development of the PS-RANSAC algorithm, which approximates the iris boundaries as non-conic entities. PS-RANSAC takes advantage of the robustness of RANSAC to noisy data and the capability of Splines for representing functions with an arbitrary number of degrees of freedom. In Choi et al. (2009), RANSAC techniques have demonstrated better accuracy in approximating series that have high signal-to-noise ratios. However, other RANSAC-based iris segmentation techniques in the literature, as in Chou et al. (2010); Wang and Qian (2011), assume a conic shape for the iris boundary, which can restrict the success of iris segmentation when dealing with non-ideal images. In our experiments, PS-RANSAC obtained important improvements in terms of accuracy and robustness to noise with respect to state-of-the-art techniques. Another valuable contribution of this paper is the experimental evaluation of the benefits of various illumination compensation algorithms on segmentation accuracy and recognition performance. This paper presents the first systematic comparison of different illumination compensation techniques on the recognition accuracy of an iris system based on a segmentation method that can effectively deal with non-ideal samples. A further contribution is the exhaustive analysis of recent techniques for overcoming non-

idealities in iris images that can degrade the performance of segmentation methods.

Experiments were conducted using three databases of non-ideal samples: the "West Virginia University Non-ideal Iris Image Database", the "Quality-Face/Iris Research Ensemble" (Q-FIRE) database , and the "Noisy Visible Wavelength Iris Image Databases v.2" database, which specifically include images exhibiting various types of nonidealities. Results show that the proposed segmentation method offers a considerable improvement in accuracy compared with other techniques presented in the literature for datasets acquired in non-ideal scenarios. The proposed method also achieved satisfactory performance on three datasets of images acquired in more favorable conditions: the CASIA-IrisV4 Interval database, the IIT Delhi Iris Database Version 1, and the ND-Iris-0405 database. Moreover, the results show that illumination compensation techniques based on the Retinex model yield better segmentation and recognition accuracy.

The paper is structured as follows. Section 2 presents related work. Section 3 describes the illumination compensation methods considered in this work and the novel segmentation strategy. Section 4 details the experiments performed and the results obtained. Section 5 presents a discussion on the achieved accuracy and Section 6 concludes the paper.

2. Related Work

The study described in Schmid et al. (2013) revealed that discarding low-quality iris samples can considerably improve recognition performance. The authors demonstrated that their proposed quality assessment method could decrease the error rate by 20 to 35 percent.

The IREX II Iris Quality Calibration and Evaluation (IQCE) competition, conducted by the National Institute of Standards and Technology (NIST) and presented in Tabassi et al. (2011), evaluated the effects of various nonidealities in iris images on the performance of an iris system. The list of characteristics that affected the results was sorted by relevance as follows: usable iris area, iris-pupil contrast, pupil shape, iris-sclera contrast, gaze angle, sharpness, dilation, interlacing, gray-scale spread, iris shape, iris size, motion blur, and signal-to-noise ratio. This study showed that characteristics related to the illumination conditions (iris-pupil contrast, iris-sclera contrast, and gray-scale spread) strongly influence the performance of iris segmentation methods.

Nonidealities in iris images caused by illumination factors can be present both in samples acquired using specialized iris scanners as well as in images acquired at a distance using commercial digital cameras. Iris scanners typically use an array of illumination sources placed in the vicinity of the eye to obtain uniformly illuminated images. In this scenario, the most important problem that arises is related to non-uniform illumination of the iris region due to incorrect positioning of the user with respect to the acquisition sensor. Images acquired at a distance can suffer from similar problems and can also present low contrast between the iris and the surrounding regions due to the large distance between the eye and the illumination source or the influence of ambient illumination. Furthermore, in natural light conditions, dark eyes present a low pupil-iris contrast and low contrast between the iris and eyelashes.

When illumination is not ideal, traditional approaches for iris segmentation can yield poor results due to the following reasons:

- the iris-sclera contrast can be low and non-uniform,
- the iris-pupil contrast can be low and non-uniform,
- the contrast between the iris and eyelashes can be low and non-uniform,
- the iris region can exhibit gray-level intensity levels similar to that of the skin, and
- the iris region can exhibit reflections.

In the literature, various studies have been presented on iris segmentation methods that are robust to samples affected by nonidealities, as in Donida Labati et al. (2012); Jillela and Ross (2014, 2013); Proenca and Alexandre (2012b). Moreover, several studies have evaluated preprocessing methods for reducing various nonidealities in iris images. Table 2 briefly reviews the methods in the literature designed to overcome specific nonidealities.

This section first provides an overview of iris segmentation algorithms designed for application to non-ideal images and then presents descriptions of various illumination compensation techniques adopted in iris recognition systems.

2.1. Iris segmentation methods

Iris segmentation includes the determination of the inner and outer iris boundaries as well as the estimation of the iris regions occluded by eyelids, eyelashes, hair, glasses and reflections. Usually, a segmentation method first estimates the iris boundaries and then refines the segmentation by removing reflections and occlusions. Table 3 presents a general overview of methods for estimating iris boundaries.

The majority of methods for segmenting iris boundaries approximate the contours as pre-defined geometric shapes, such as circles or ellipses. One segmentation method that is widely used in iris recognition systems was presented in Daugman (2002). To define both the inner and outer iris boundaries, this method uses the integro-differential operator (IDO) that searches for a circular contour with maximum variation in intensity across its boundary in the radial direction. It also searches for the boundaries of the eyelids by changing the shape of the integral path from circular to arcuate. Many variants of this method have been presented in the literature, some of which are designed to search for elliptical shapes, like in Shamsi and Kenari (2012). An example of an algorithm designed to reduce the computation time of the IDO method is the "intDiff" constellation, presented in Tan et al. (2010).

The technique based on the Hough transform described in Wildes (1997) is also very popular. This technique searches for pre-defined parametrized shapes by applying a voting procedure that analyzes the edges extracted from the input image. Because of its simplicity and robustness to noisy data,

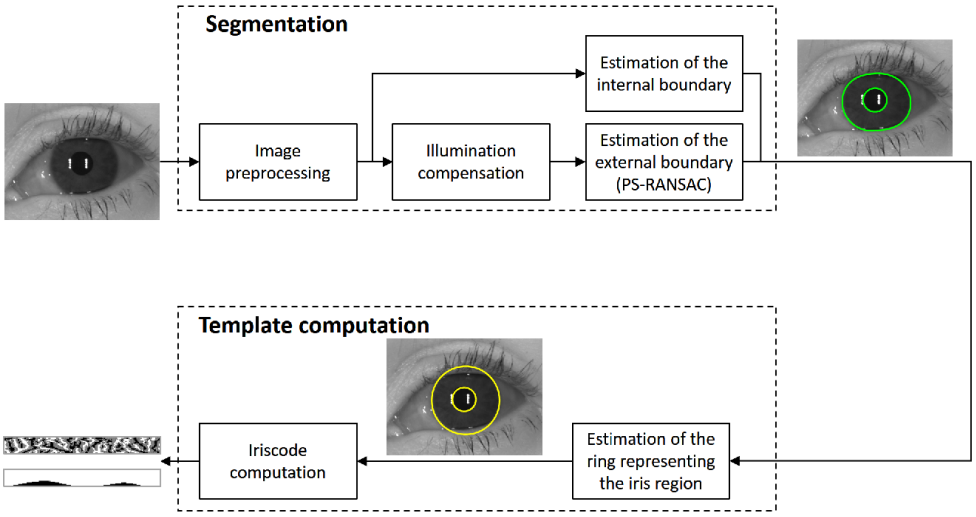

Fig. 4. Schema of the segmentation and template computation tasks of the iris recognition process.

it has been widely used in the literature. The techniques described in Feng et al. (2006); Masek and Kovesi (2003) present Hough-transform-based methods that search for circular shapes and the work proposed in Zuo and Schmid (2010) presents a Hough-transform-based method that searches for elliptical shapes. Moreover, some segmentation methods apply the Hough transform after invoking a pre-processing step intended to reduce both the level of noise and the area to be searched in an iris image. For example, the method described in Proença and Alexandre (2006) applies region clustering before boundary segmentation.

Methods based on the RANSAC algorithm strive to achieve greater robustness to nonidealities in iris images. RANSAC is an iterative method for curve fitting based on data that contain outliers. For particularly noisy data, this method can usually achieve better results than the Hough transform. The work presented in Chou et al. (2010) uses RANSAC to refine the iris boundaries obtained using classifiers that select contour points from features extracted from four-spectral images. Similarly, in Wang and Qian (2011), RANSAC is used to refine the boundaries obtained using linear basis functions in the polar coordinate system. The method presented in Morley and Foroosh (2017) uses a version of RANSAC with a modified metric distance to estimate a circle approximating the pupil boundary from features extracted using a deep Convolutional Neural Network (CNN). The RANSAC algorithm has also been used to segment the eyelids in Chou et al. (2010); Li et al. (2010); Liu et al. (2009).

Other interesting techniques for approximating iris boundaries based on previously defined shapes include the "Pulling and Pushing" method presented in He et al. (2009) and "Starburst" method described in Ryan et al. (2008).

To reduce the noise present in iris templates, recent articles have studied segmentation methods that are able to extract the iris boundaries without requiring any assumption about their shapes. Such iris segmentation methods can be divided into the following categories: approaches based on active contours, incremental methods, methods based on analysis of local characteristics, and methods based on deep learning.

Many approaches reported in the literature for the segmentation of poor-quality iris images involve the computation and analysis of local characteristics of an iris image to enable the labeling of different regions using clustering or classification methods. In most cases, this computation is a preliminary step with the purpose of reducing the search area and decreasing the amount of noise. Examples include Tan et al. (2010); Proença and Alexandre (2006); Li et al. (2010); Proença (2010); Du et al. (2011). Some studies have also investigated segmentation techniques that use computational intelligence to locate only those pixels that describe the iris region, as in Broussard et al. (2007). The study in Zhao and Kumar (2015) presents a total-variation based formulation which uses L1 norm regularization to robustly suppress noisy texture pixels for the accurate iris localization.

Segmentation methods that are based on active contours iteratively adapt the segmented shape to the edges extracted from the image. One well-known method of this type was presented in Shah and Ross (2009); Ross and Shah (2006). In each iteration, the curve that describes the iris boundary evolves toward the edges of the iris contour based on an evaluation of the Thin Plate Spline energy to analyze the relation between the active contours and the geodesics (curves of minimal length). Another active contour method is proposed in Zhang et al. (2010) that uses a different distance measure, called the semantic iris contour map. The method presented in Abdullah et al. (2017) introduces an external force to the active contour model to robustly segment non-ideal samples. In Jillela et al. (2013), active contours have also been used to segment the iris region in periocular images.

In incremental methods, an initial approximation of the iris shape is first obtained, and refinement algorithms are then applied to represent the iris boundaries as two closed curves with arbitrary degrees of freedom. The method described in Daugman (2007) first computes a simple preliminary estimation of the iris center by applying the IDO method. Then, it searches for points on the contours by selecting the pixels that corre-

Table 2. State of the art for addressing nonidealities in iris recognition.

nonideality	Studies in the literature
Occlusions	Iris segmentation – Proenca and Alexandre (2012a); Jillela et al. (2013); Donida Labati et al. (2012)]
Poor focus	Focus compensation – Kang and Park (2005); He et al. (2008a); Boddeti and Kumar (2008); Kang and Park (2007) Super-resolution – Nguyen et al. (2011, 2012, 2010)
Low resolution	Image reconstruction – Alonso-Fernandez et al. (2015)
Gaze deviation	Gaze adjustment – Daugman (2007); Kennell et al. (2009); Yang et al. (2014)
Pupil dilation	Dilation compensation – Tomeo-Reyes et al. (2015); Thornton et al. (2007); Hollingsworth et al. (2009)
Reflections	Reflection detection – Zuo and Schmid (2010); Ross and Shah (2006); Scotti and Piuri (2010); Li and Savvides (2013)
Natural light illumination	Iris segmentation – Proenca and Alexandre (2012a); Tan et al. (2010); Donida Labati and Scotti (2010); ho Cho et al. (2006) Feature extraction and matching – Bowyer (2012); Raja et al. (2015); Marsico et al. (2014)
Poor infrared illumination	Illumination compensation – Jillela and Ross (2013); Jillela et al. (2013); Shukri et al. (2013); Tan and Kumar (2013)

spond to the maximum values of the gradient computed in the radial direction with respect to the iris center. In the final step, the contour points are fitted using an algorithm based on the computation of the m coefficients of a discrete Fourier series. In the methods described in Donida Labati et al. (2009a,b), boundary refinement is performed in a similar manner, but additional noise reduction strategies are applied to cope with non-ideal iris images. Another incremental method is described in Tan and Kumar (2013). This approach exploits a random walker algorithm to coarsely estimate the iris region and then uses a sequence of algorithms designed to enhance the segmentation accuracy.

Recent methods based on deep learning techniques obtained remarkable segmentation accuracy for different image datasets. However, these methods require long training time and need a fine tuning to obtain the best performance in heterogeneous scenarios. The study presented in Liu et al. (2016) does not use any preprocessing or postprocessing strategy and includes two segmentation techniques based on different topologies of CNNs (hierarchical convolutional neural networks and multi-scale fully convolutional networks). The method presented in Arsalan et al. (2017) roughly estimates the iris region using an edge detection algorithm and then classifies the pixels in two classes (iris and non-iris) by using a CNN. The paper performed a fine tuning of a VGG CNN, similarly to Parkhi et al. (2015), for iris images acquired in visible light conditions. The method presented in He et al. (2017) consists of a specifically designed CNN able to classify every pixel into the following classes: pupil, iris, sclera, and background. The studies presented in Jalilian and Uhl (2017); Jalilian et al. (2017) use a fully convolutional encoder-decoder network trained for classifying iris and non-iris pixels in images acquired in a wide set of heterogeneous conditions. Convolutional encoder-decoder networks are also used in Sinha et al. (2017) to classify pixels pertaining to the pupil, iris and background. The work presented in Arsalan et al. (2018) proposed a deep network called IrisDenseNet and based on VGG-16 Simonyan and Zisserman (2014). The work presented in Bazrafkan et al. (2018) proposes a deep CNN and a data augmentation method for making the training process robust to heterogeneous non-ideal conditions. The work described in Morley and Foroosh (2017) uses a CNN to extract the edges of the limbic boundary. Other studies employ deep learning strategies for the feature extraction and matching steps of the iris recognition system, as in Gangwar and Joshi (2016); Zhao and Kumar (2017).

After estimating the iris boundaries, segmentation methods typically remove reflections using algorithms that analyze statistical indices computed based on the image intensity, as in Zuo and Schmid (2010); Ross and Shah (2006). Several studies have also investigated methods based on classification techniques and more complex features, as in Scotti and Piuri (2010). The eyelashes can be segmented using algorithms based on features obtained by applying various techniques: Donida Labati and Scotti (2010) use Gabor filters Donida Labati and Scotti (2010). He et al. (2008b) apply one-dimensional rank filters; and Aligholizadeh et al. (2011) apply wavelet transforms. An interesting approach designed to remove the occlusions caused by eyelids, eyelashes and reflections in a single step was proposed in Li and Savvides (2013). This method is based on Gaussian Mixture Modeling classifiers.

2.2. Illumination compensation for iris images

Illumination compensation techniques are widely used in biometric systems based on traits different from the iris, such as the face, as described in Makwana (2010).

The Retinex model is widely used in the literature to reduce problems related to poor illumination conditions in a wide range of application scenarios. Illumination compensation techniques based on the Retinex model attempt to improve the brightness and color consistency, thereby imposing consistency of perceived color and brightness on images that exhibit spatial and spectral variations in illumination. Specifically, the Retinex theory attempts to model the manner in which the human visual system perceives color. This theory states that an image I can be modeled as the product of a reflectance function R and a luminance function L, as follows:

$$I(x, y) = R(x, y)L(x, y). \tag{1}$$

The reflectance R represents the objects present in the image and depends on the reflectivity of each surface, whereas the luminance L describes the illumination of the scene. Illumination normalization is performed by estimating the reflectance R, which is invariant with respect to illumination conditions. This computation is performed based on manipulations of Eq. (1), as follows:

$$R(x, y) = I(x, y)/L(x, y), \tag{2}$$

Table 3. Iris segmentation methods in the literature. See Jillela and Ross (2013) for a detailed taxonomy.

Iris shape	Technique	Selected references
Circular or Elliptical	Integro-Differential Operator	Daugman (2002); Shamsi and Kenari (2012); Tan et al. (2010)
	Hough Transform	Feng et al. (2006); Masek and Kovesi (2003); Zuo and Schmid (2010); Proença and Alexandre (2006)
	RANSAC	Chou et al. (2010); Wang and Qian (2011)
	Other Techniques	He et al. (2009); Ryan et al. (2008)
Non-conic	Computational Intelligence	Tan et al. (2010); Proença and Alexandre (2006); Li et al. (2010); Proença (2010); Du et al. (2011); Broussard et al. (2007)
	Active Contours	Shah and Ross (2009); Ross and Shah (2006); Zhang et al. (2010); Jillela et al. (2013)
	Incremental Methods	Donida Labati and Scotti (2010); Daugman (2007); Donida Labati et al. (2009a,b); Tan and Kumar (2013)
	Deep Learning	Liu et al. (2016); Arsalan et al. (2017); He et al. (2017); Jalilian and Uhl (2017); Jalilian et al. (2017)

$$\ln[R(x,y)] = \ln[I(x,y)] - \ln[L(x,y)], \tag{3}$$

where Eq. (3) represents the logarithmic reflectance and Eq. (2) represents the quotient reflectance.

Methods that use the logarithmic reflectance and methods that use the quotient reflectance can both be found in the literature. Examples of methods based on the logarithmic reflectance representation include: the Single-Scale Retinex (SSR), described in Jobson et al. (1997); and Multiple-Scale Retinex (MSR), described in Jobson et al. (1997). Examples of methods based on the quotient reflectance include: the Quotient Image (QI), described in Shashua and Riklin-Raviv (2001); and Self-Quotient Image (SQI), described in Wang et al. (2004). The luminance L is usually estimated before the estimation of R by smoothing the image space I. Various methods have been studied for the optimal estimation of L for different types of images acquired under different environmental conditions.

One widely used illumination compensation method is SSR, in which L is computed by applying a Gaussian smoothing filter that is tuned according to the characteristics of the image I. When properly tuned this algorithm can obtain satisfactory results for various kinds of images. However, in the presence of strong shadows, the reflectance images often exhibit halo effects.

MSR strives to overcome this limitation. For n_g reflectance images R_i obtained using Gaussian filters with different kernels k_i, the reflectance image R is computed as follows:

$$R(x,y) = \sum_{i=1}^{n_g} R_i(x,y). \tag{4}$$

Thus, the image I is convolved with a smoothing mask, using weighting coefficients obtained by combining two measures of the illumination discontinuity at each pixel.

A different approach is used in the QI method, in which the luminance L is estimated from a set of training images. The SQI method is a variant of the QI method that is designed to estimate L directly from the image I. This estimation is performed by applying an anisotropic smoothing filter to I. One advantage of this illumination compensation method is that it reduces the presence of shadows.

Illumination compensation techniques based on the Retinex model, however, require proper tuning of their parameters to achieve satisfactory results.

Other illumination compensation methods used for biometric applications do not aim to maintain the color consistency and are based on different algorithms. Since illumination variations mainly lie in the low-frequency band, the method described in Chen et al. (2006) truncates the first coefficients of the Discrete Cosine Transform (DCT) in the logarithmic domain. The algorithm presented in Tan and Triggs (2010) is composed of the following steps: gamma correction, Difference of Gaussian (DoG) filtering, masking, and contrast equalization. In the following, we will refer to these techniques as DCT and TT, respectively.

Only a few iris recognition methods presented in the literature use preprocessing algorithms that are specifically designed for illumination compensation. In fact, most existing systems include an enhancement step that simply improves the image contrast. Commonly used techniques for this purpose are based on well known image processing algorithms described in Gonzalez and Woods (2006) and include histogram equalization, local histogram equalization, adaptive histogram equalization and gamma correction. However, these techniques cannot address all nonidealities caused by illumination conditions; they typically yield poor results in the presence of non-uniform illumination, strong shadows and reflections. Moreover, most of these techniques rely on certain assumptions regarding the histogram distribution and use a set of fixed thresholds and parameters; therefore, images with similar characteristics and of similar resolutions are required to obtain satisfactory results.

The method presented in Shah and Ross (2009) uses an illumination compensation technique based on the anisotropic nonlinear diffusion. Other studies use algorithms based on the Retinex model. There are also studies that use Single Scale Retinex (SSR), as in the case of the methods described in Tan and Kumar (2013, 2012); Zhao and Kumar (2015). The work in Shukri et al. (2013) presents a more complete study that includes both Single and Multi Scale Retinex (MSR) applied to UBIRIS dataset. However, the study uses segmentation algorithm presented in Masek and Kovesi (2003), which is not designed for non-ideal iris images. In addition, the article does not provide information about the parameters used by the illumination compensation algorithms and uses subjective figures of merit. In contrast, our paper presents the first systematic comparison of different illumination compensation techniques by evaluating the recognition accuracy of a system based on a segmentation method effectively able to deal with non-ideal samples.

3. The Proposed Approach

We propose a novel iris segmentation method that is designed to overcome the various nonidealities observed in poor-quality iris images acquired under challenging infrared or visible light

illumination conditions. This method can be divided into the following sequential steps:

A) image preprocessing,

B) estimation of the internal iris boundary,

C) illumination compensation, and

D) estimation of the external iris boundary (PS-RANSAC).

Because most feature extraction and matching algorithms presented in the literature normalize the iris area by assuming that the limits of the internal and external iris boundaries can be represented by two circles or ellipses, we also propose an algorithm for estimating such limits from the segmented areas obtained using our method. This segmentation algorithm generates a circular approximation of the external limit of the iris region by evaluating the boundaries of the segmented iris mask.

Appendix A reports details on the parameters of the proposed algorithms and on tests performed to evaluate their robustness with respect to a wide range of different values, showing satisfactory results.

3.1. Image preprocessing

The purpose of this step is to eliminate details in an iris image that can reduce the iris segmentation accuracy, and the procedure used for this purpose is specifically designed for the proposed iris segmentation algorithms. Furthermore, in case of a color image, this step extracts only the red channel from the input iris image. The computation can be divided into two tasks: the removal of specular reflections and noise reduction.

To remove specular reflections, a binary map B of the reflection regions is first computed by analyzing the response of the iris image I_{in} to Gabor filters tuned using an empirically estimated frequency f. First, the images G_0 and G_{90} are computed by convolving I_{in} with Gabor filters with orientations of 0° and 90°, respectively. Then, an image describing the reflections, I_R, is computed from G_0 and G_{90}. Subsequently, a binary map of the reflection regions, B_R, is obtained from I_R, and the reflections are removed using the inpainting algorithm described in Bertalmio et al. (2000). The image I_R is calculated as follows:

$$I_R(x, y) = G_0(x, y) + G_{90}(x, y). \tag{5}$$

The binary image B_R is computed as follows:

$$B_R(x, y) = \begin{cases} 1 & \text{if } I_R(x, y) > t_R \\ 0 & \text{otherwise} \end{cases}, \tag{6}$$

where t_R corresponds to the p_R percentile of I_R. The value of p_R is empirically tuned on the dataset(s) to be analyzed.

Then, the noise is reduced by applying a Gaussian-based bilateral filter to I_R , as described in Paris et al. (2009). Bilateral filters are non-linear algorithms that allow an image to be blurred while preserving strong edges.

For an image I, the notation I_p represents the intensity of I at pixel p. Similarly, I_q is the intensity of I at pixel q. The bilateral filter $BF[\cdot]$ is defined as follows:

$$BF[I]_p = \frac{1}{W_p} \sum_{q \in S} G_{\sigma_s}(\|p - q\|)\, G_{\sigma_r}\left(I_p - I_q\right) I_q, \tag{7}$$

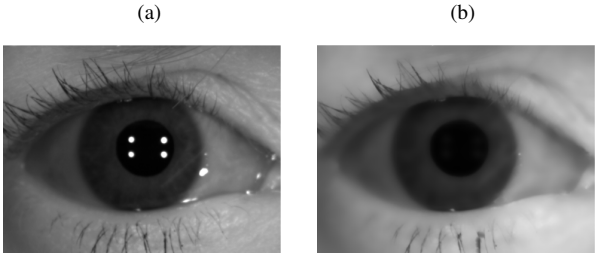

Fig. 5. Example of the results obtained using the proposed preprocessing: (a) the input image I and (b) the processed image. The output image is less affected by noise and specular reflections than is the input image, and simplify the segmentation process.

where W_p is a normalization factor that ensures that the pixel weights sum is in the range $1 : 0$ and is computed as follows:

$$W_p = \sum_{q \in S} G_{\sigma_s}(\|p - q\|)\, G_{\sigma_r}\left(I_p - I_q\right). \tag{8}$$

Here, S is the set of all possible locations in the image (the spatial domain), G_{σ_s} is a spatial Gaussian kernel that decreases the influence of distant pixels, and G_{σ_r} is a range Gaussian kernel that decreases the influence of pixels q with an intensity value different from I_p. The Gaussian kernels G_{σ_s} and G_{σ_r} have standard deviations of σ_s and σ_r, respectively. The values of σ_s and σ_r and the size of the filter ($S = N_q \times N_q$ pixels) are empirically tuned on the dataset(s) to be analyzed.

We apply a bilateral filter to compute the enhanced image I_R as follows:

$$E = BF[I_R]_p. \tag{9}$$

Fig. 5 presents an example of a degraded iris image before and after the application of the proposed preprocessing technique. The preprocessed image is less affected by noise and specular reflections than the input image.

3.2. Estimation of the internal iris boundary

We present a novel iterative algorithm optimized to deal with iris images affected by strong differences in illumination conditions and low iris-pupil contrast. The algorithm improves the robustness to irregularly shaped boundaries affected by noise and reflections by mixing an iterative thresholding technique designed for searching circular shapes and a RANSAC-based technique designed to regularize the pupil shape by discarding possible outliers.

The internal iris boundary is extracted from a binary image representing the pupil region. This image is computed by iteratively searching for the most circular shape obtained when binarizing the iris image in an empirically estimated range of intensity thresholds.

In each iteration i, a binary image B_i is computed by applying a threshold value $T(i)$ to the image E. The 8-connected regions with major axis lengths greater than l_{min} and less than l_{max} are then identified as candidate pupil regions. Of these 8-connected regions, the region with the minimum eccentricity is ultimately chosen as the pupil area.

The coordinates of the pupil boundary are then extracted and refined using RANSAC for circle fitting, thus obtaining the vector of points v_B.

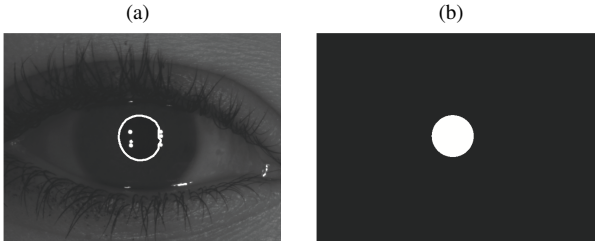

Fig. 6. Example of the results obtained using the proposed algorithm for the estimation of the internal iris boundary: (a) the identified pupil area and (b) the corresponding binary mask obtained from the refined boundary points v_B.

For color images, which frequently present low iris-pupil contrast and dark eyelids and eyelashes, intensity-based algorithms frequently estimate the pupil region as part of the eyelashes. For this reason, works in the literature frequently perform a rough estimation of the external iris boundary to limit the image region candidate to represent the pupil, as in Proenca and Alexandre (2012a). Therefore, we narrowed the search region by using the integro-differential operator described in Daugman (2002), which is sufficiently effective in estimating the external iris boundary. In fact, color images usually present a high iris-sclera contrast, thus permitting to estimate the iris region reasonably well. However, this operator usually obtains poor accuracy in estimating the internal iris boundary. We, therefore, apply the proposed pupil segmentation algorithm in a region of interest corresponding to a circle with radius equal to $1/3$ of the radius estimated by applying the integro-differential operator for searching the external boundary. We experimentally proved that the version of algorithm designed for iris images acquired in infrared illumination failed for the great majority of the images acquired in natural light illumination and depicting dark eyes due the fact that contrast of eyelids and eyelashes with the skin is much higher with respect to the pupil-iris contrast. Similarly, we experimentally proved that the version of the algorithm designed for iris images acquired in natural light illumination failed for most of the images acquired using infrared illuminators because the integro-differential operator described in Daugman (2002) detects edges with higher contrast with respect to the iris-sclera boundary.

An example of an estimated pupil area and the corresponding boundary points v_B are presented in Fig. 6.

3.3. Illumination compensation

The proposed method exploits a specific Illumination compensation algorithm to improve the robustness of the subsequent steps to estimate the outer external iris boundaries with different light bandwidths and in the presence of nonidealities. We studied various illumination compensation techniques to determine which algorithm was the best to improve the iris segmentation accuracy and, thus, the overall performance of the iris recognition system. This study considered both non-ideal images acquired using traditional NIR iris scanners and color images captured using digital cameras placed at different distances from the subject. In this context, we considered the following approaches:

1. histogram equalization;
2. analysis of the histogram distribution;
3. local histogram analysis;
4. transformations of the image intensity, such as logarithmic, square-root, and exponential transformations;
5. algorithms based on the Retinex model, such as SSR and MSR; and
6. other algorithms that are commonly used for face recognition, like SQI, DCT, and TT.

In the following, we will refer to the image R_E as the one obtained by applying an illumination compensation strategy algorithm $F_{I,L}(\cdot)$ to E. As an example, for the algorithm SSR, $R_E = E/L$.

We performed extensive tests to investigate the effect and details of every algorithms. A Section 4.5 reports a detailed descriprion of the obtained results.

Fig. 7 shows some examples of the results of the best-performing techniques.

3.4. Estimation of the external iris boundary (PS-RANSAC)

This step involves estimating the points on the external iris boundary by searching for the maximum values obtained when a radial-gradient-based operator is applied to the image R_E and refining the boundary shape using our variant of RANSAC.

The first task consists of estimating the vector of the external boundary points, E_B, from the image R_E and is performed by searching for the coordinates of the points at which the maximum values are obtained when a gradient-based operator is applied in polar coordinates.

An image I_P is computed by converting R_E into polar coordinates with the center at the centroid of the pupil and with a radial resolution of 1° (360 columns). Because the internal iris boundary is typically characterized by a higher contrast than the external boundary, the image I_P is computed starting at a minimum radius r_{min}, which is empirically tuned on the dataset(s) to be analyzed.

Our gradient-based operator is applied to enhance the visibility of the continuous segments describing the iris boundary. This operator is designed to reduce the hindrance posed by eyelids to traditional gradient-based approaches and is computed as follows:

$$I_G(\theta,\rho) = I_P(\theta,\rho) * m(\theta',\rho'), \tag{10}$$

where m is a $4 \times N$ mask defined as follows:

$$m(\theta',\rho') = \begin{cases} 1 & \text{if } y_m > 2, \\ 0 & \text{otherwise,} \end{cases} \tag{11}$$

where y_m is the y coordinate of the mask m and $*$ is the convolution operator.

For each angle θ, the corresponding radius is computed as follows:

$$X(\theta) = \underset{\rho=1\ldots P}{\operatorname{argmax}} \left[I_G(\theta,\rho) \right], \tag{12}$$

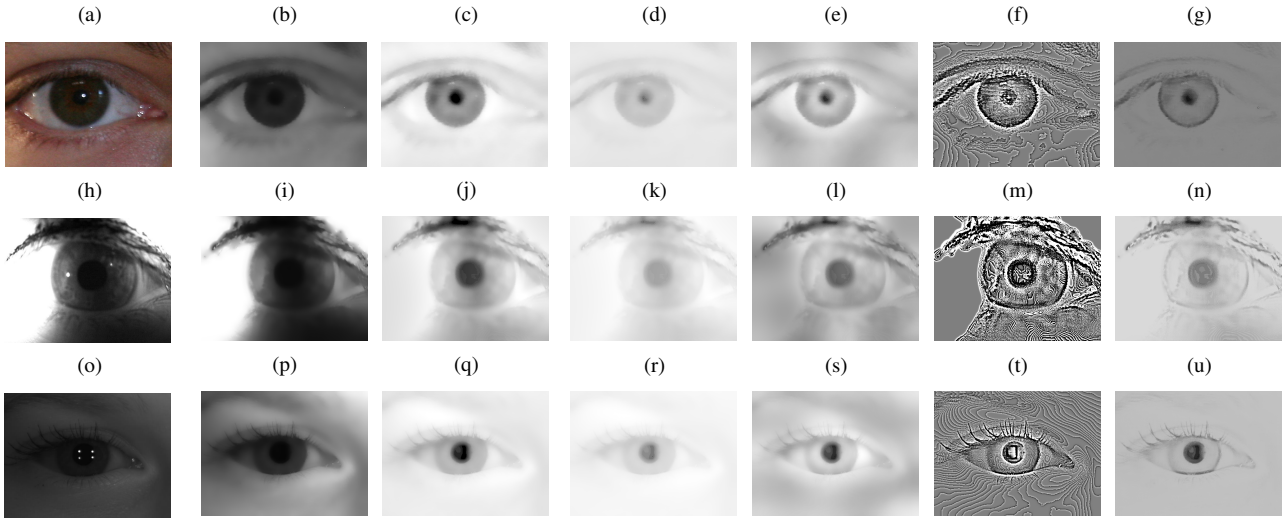

Fig. 7. Examples of illumination compensation techniques applied to an image from DB UBIRIS v2 dataset (first row), DB WVU (second row) and DB QFIRE (third row) : (a, h, o) input image I, (b, i, p) enhanced images E, (c, j, q) E after SSR processing, (d, k, r) E after MSR processing, (e, l, s) E after DCT processing, (f, m, t) E after TT processing, (g, n, u) E after SQI processing. The illumination compensation mitigates problems caused by non-uniform illumination, increasing the contrast between pupil and iris, and delimiting better the iris with respect to eyelids and sclera. TT and SQI introduce some artificial edges and artifacts that may hinder their performance. SSR, MSR, and DCT mitigate problems caused by non-uniform illumination. With respect to SSR and DCT, MSR reduces the iris-sclera contrast but increases the iris-eyelid contrast and reduces the visibility of eyelashes, thus simplifying the segmentation of the most challenging image regions.

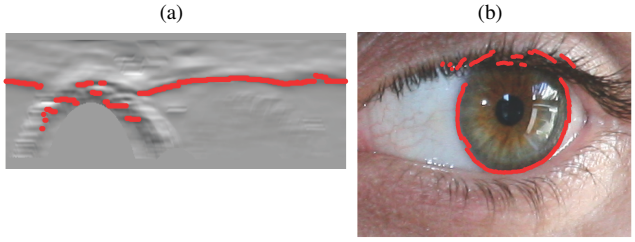

Fig. 8. Boundary estimation using our proposed PS-RANSAC algorithm: (a) boundary points in polar coordinates and (b) boundary points in Cartesian coordinates. The proposed gradient-based operator enhance the visibility of the continuous segments describing the iris boundary.

where P is the size of the image I_G along the ρ axis. Fig. 8 presents an example of an estimated external boundary X.

The second task in our method for external boundary segmentation consists of refining the shape of the estimated iris contour by applying our RANSAC-based algorithm, as described in the following.

In segmentation applications, RANSAC and the proposed PS-RANSAC can be used to fit a set of candidate boundary points by discarding outliers. The iris segmentation methods presented in the literature use the well-known versions of RANSAC designed for circle or ellipse fitting, as in Chou et al. (2010); Wang and Qian (2011); Li et al. (2010). Unlike these methods, PS-RANSAC approximates the iris boundaries as closed curves with arbitrary degrees of freedom.

PS-RANSAC can be divided into the following steps:

1. Select a set of n_p "hypothetical inliers" X_I from the set of input points X.

2. Fit an approximating function $a_f(\cdot)$ to the set of "hypothetical inliers" X_I.

3. Use all other points in X to evaluate the accuracy of the computed approximating function by computing an error metric. The points that are fitted with an error distance that is equal to or less than a certain threshold value t_f are considered to be part of the "consensus set".

4. The algorithm terminates when the "consensus set" exhibits a fitting error equal to or less than a certain threshold value t_e or when the maximum number of iterations i_{max} is reached.

Unlike the RANSAC algorithms for circle or ellipse fitting, which use boundary representations in Cartesian coordinates, PS-RANSAC considers iris boundary points that are expressed in polar coordinates, (θ,ρ). To guarantee the closure of the fitted function in Cartesian coordinates, the n_p "hypothetical inliers" are replaced twice, in the ranges $[-2\pi,\ldots,0]$ and $[-2\pi,\ldots,4\pi]$. The approximating function $a_f(\cdot)$ (step 3) that is used by PS-RANSAC consists of a spline of arbitrary order N. The error metric (step 4) that is computed by PS-RANSAC is the absolute distance between the points of the "consensus set" X_C and the points obtained by fitting the spline $a_f(\cdot)$ in the corresponding θ coordinates (in the range from 0 to 2π). Finally, the points are transformed into Cartesian coordinates to yield the set of refined external boundary points, E_R.

Algorithm 1 presents the pseudo-code for PS-RANSAC. Fig. 9 shows an example of the results of applying the boundary refinement process to the points shown in Fig. 8.

3.5. Estimation of the circles representing the limits of the iris region

In the proposed iris segmentation approach, the iris boundaries are described by curves with arbitrary degrees of freedom. However, traditional iris recognition systems, like the

Algorithm 1 Pseudo-code for PS-RANSAC

function PS-RANSAC(X, N, t, i_{max})
  ▷ X is a set of polar coordinates
  ▷ t is the error threshold
  ▷ N is the order of the approximating spline
  ▷ i_{max} is the maximum number of iterations

  $i \leftarrow 0$ ▷ Iteration counter
  $b_E \leftarrow \infty$ ▷ Best error
  $b_S \leftarrow \infty$ ▷ Best spline
  while $(i < i_{max})$ **or** $(b_E > t)$ **do**
    $n_p \leftarrow N + 1$ ▷ ♯ of "hypothetical inliers"
    $X_I \leftarrow$ SelectPoints(X, n_p) ▷ Random selection
    $s_I \leftarrow$ PolarSpline(X_I, N) ▷ Spline of order N
    $R_I \leftarrow$ EvalSpline(X, s_I) ▷ Fitted points
    $D_I \leftarrow |X[2,:] - P_I|$ ▷ Fitting error
    $C_I \leftarrow$ find$(D_I \leq t_f)$ ▷ "Consensus set"
    $i_N \leftarrow$ length(C_I) ▷ Size of the "Consensus set"
    if $\sum(D_I) \geq b_E$ **then**
      $b_E \leftarrow \sum(D_I)$ ▷ Update the best error
      $b_S \leftarrow S_I$ ▷ Update the best spline
return b_S

function PolarSpline(X')
  ▷ X' is a set of polar coordinates
  $\Theta \leftarrow X'[1,:]$ ▷ θ coordinates
  $P \leftarrow X'[2,:]$ ▷ ρ coordinates
  $\Theta_T \leftarrow [(\Theta - 2\pi), \Theta, (\Theta + 2\pi)]$ ▷ Concatenation
  $P_T \leftarrow [P, ¶, ¶]$ ▷ Concatenation
  s = spline(Θ_T, P_T) ▷ Curve fitting
return s

one described in Daugman (2002), require the iris region to be delimited by two circles for the subsequent computation of a scale-invariant representation of the iris region (Rubber Sheet Model).

To be used in these systems, the proposed method estimates the internal iris boundary as a circle from the shape describing the external iris boundary.

To provide a robust representation of the iris shape, our algorithm discards points corresponding to the contours of the eyelids and eyelashes from the vector E_R, which represents the refined coordinates of the external boundary, and then performs circle fitting based on the mean-square approach using the remaining coordinates and hence the algorithm considers only those points in E_R with θ coordinates in the ranges $[-10°, \ldots, 40°]$ and $[140°, \ldots, 90°]$.

4. Experimental Results

We evaluated the accuracy of the proposed algorithms in the following scenarios:

1. non-ideal samples captured using digital cameras placed at different distances from the eye and in different infrared illumination conditions;

2. non-ideal samples acquired using commercial iris scanners;

3. non-ideal samples captured in natural light illumination and on the move;

4. and samples acquired using commercial iris scanners in controlled conditions.

The considered samples exhibit large differences in resolution (the iris radius varies from 110 pixels to 300 pixels) and are

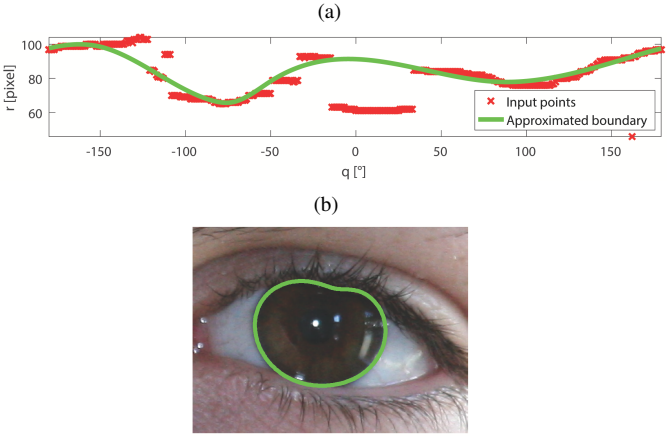

Fig. 9. Boundary refinement using our proposed PS-RANSAC algorithm: (a) input and output points in polar coordinates and (b) the external iris boundary in Cartesian coordinates. The proposed approach reduces irregularities in the estimated boundary and removes possible outliers.

affected by the following nonidealities: poor illumination, occlusions, gaze deviation, motion blur, poor focus, reflections, and frame interlacing.

First, we analyzed the performance of the proposed segmentation approach for each of the four scenarios by comparing the achieved results with that of state-of-the-art techniques. Second, we experimentally evaluated the effects of different illumination compensation techniques on the segmentation accuracy and performed preliminary tests to evaluate the effects of illumination compensation on the feature extraction. Third, we analyzed the computational time required by the proposed algorithms.

4.1. Datasets

We evaluated the accuracy of the proposed method for 6 heterogeneous datasets.

4.1.1. DB QFIRE

is composed of non-ideal samples captured using digital cameras placed at different distances from the eye and in different infrared illumination conditions. It is a subset of the "Quality-Face/Iris Research Ensemble" (Q-FIRE) database, described in Johnson et al. (2010). Q-FIRE was conceived as a benchmark to evaluate quality assessment algorithms and was the dataset used in the NIST Iris Quality Calibration and Evaluation (IQCE) competition, presented in Tabassi et al. (2011), in which the major players in the biometric market participated. The results of this competition illustrate the challenge that represents this dataset, since the most important commercial algorithms could not process many of the samples that we use in our tests. To the best of our knowledge, this is the first work that studies segmentation or recognition methods able to deal with the samples of this challenging dataset.

In this work we define DB QFIRE as a set of 2598 images selected from the Visit 1 subset of the Iris Illumination set in the Q-FIRE database, which contains 1350 frame sequences representing portions of faces, each depicting either one or two eyes of one of 90 individuals. The frame sequences contain a total

of 202, 435 frames depicting both open and closed eyes and exhibiting large differences in focus. We selected the iris regions of a single frame for each one of the 1350 frame sequences belonging to the Iris Illumination set of Q-FIRE Visit 1. We extracted a single frame from each of the frame sequences representing different illumination conditions. Frame selection was performed by choosing the image with the best focus, which is considered as a standard procedure in real biometric systems, as described in Daugman (2002). Because the primary focus of this paper is iris segmentation from the ocular region, we manually performed an intial localization of the irises in the face images. Left and right iris images were manually cropped from the selected frames by selecting an area of 640×480 pixels centered on the pupil. We selected only frames that contained complete iris regions. Because of licensing agreements, we cannot directly release the images contained in the dataset. To permit the reproducibility of the performed tests, we report the frame number and cropping coordinates for each cropped iris image on our laboratory website. Donida Labati et al. (2019) provides a link to the data. Using this information, DB QFIRE can be easily reconstructed from the public Q-FIRE database.

The samples were captured using a digital camera and present appositely introduced nonidealities, such as strong illumination problems, gaze deviation, and occlusions. The camera was placed at different distances from the subjects (5 ft, 7 ft, 11 ft, 15 ft, 25 ft), under different illumination conditions (low, medium, and high), and while adjusting the focus ring of the lens from its lowest limit to infinity. The obtained iris images exhibit various nonidealities, such as occlusions, differences in illumination, large differences in iris diameter (from approximately 110 pixels to more than 300 pixels), and different kinds of specular reflections (reflections from windows and highlights on contact lenses, glasses and the corneal surface). Fig. 2 presents examples of images captured under different illumination conditions and at different distances.

There are no segmentation masks publicly available for this dataset.

4.1.2. DB WVU

is composed of non-ideal samples acquired using commercial iris scanners. It consists of all the images included in the "West Virginia University Non-ideal Iris Image Database", described in Crihalmeanu et al. (2007). These images were captured appositely performing low quality acquisitions. Many studies consider WVU as a very challenging dataset for iris segmentation, as in Yang et al. (2014); Du et al. (2011); Nguyen et al. (2010); Land (1977); Jobson et al. (1997); Jobson et al. (1997). Due to the challenging images, most of the studies using WVU dataset do not report the recognition accuracy on the overall set of images, as in Du et al. (2011); Yang et al. (2014); Land (1977); Jobson et al. (1997); Jobson et al. (1997).

DB WVU includes 3099 images representing the left and right eyes of 240 subjects. The size of the iris images is 640 × 480 pixels.

The samples were acquired using the scanner OKI Irispass-h. The iris images exhibit various nonidealities, such as occlusions (Fig. 1 a), poor illumination (Fig. 1 b), blur (Fig. 1 c), gaze deviations (Fig. 1 d), pupil dilation (Fig. 1 e), and interlacing (Fig. 1 f). Fig. 1 presents examples of images acquired appositely performing low quality acquisitions.

There are no segmentation masks publicly available for this dataset.

4.1.3. DB UBIRIS v2

is composed of non-ideal samples captured in natural light illumination and on the move. It is a subset of the second version of the "Noisy Visible Wavelength Iris Image Databases" (UBIRIS v.2), described in Proenca et al. (2010). This database is considered as challenging by many works in the literature, as in Proenca and Alexandre (2007).

In this work we define DB UBIRIS v2 as a set of 2250 samples for which manually segmented masks are publicly available, as described in Hofbauer et al. (2014). The images correspond to left and right eyes, have been captured in visible light and under unconstrained conditions and have a size of 400×300 pixels. The acquisitions have been performed on-the-move at distances varying from 4 to 8 meters from the camera.

The ocular images contain important nonidealities, such as occlusions, reflections, off-angle and blur. Fig. 3 presents examples of non-ideal images acquired using a digital single-lens reflex digital camera in an uncooperative scenario, at different distances from the camera, and in natural light conditions.

In our tests, we considered as ground truth the masks manually segmented by Operator A, as described in Hofbauer et al. (2014).

4.1.4. DB CASIA 4i

is composed of samples acquired using commercial iris scanners in controlled conditions. It a is subset of "CASIA-IrisV4 Interval" database (The Center of Biometrics and Security Research).

In this work we define DB CASIA 4i as a set of 2.639 samples corresponding to the left and right eyes of 249 subjects, for which manually segmented masks are publicly available, as described in Hofbauer et al. (2014). The images correspond to left and right eyes and have a size of 320 × 280 pixels. To directly compare the results of our method with other recent studies in the literature, we also created a subset DB CASIA v4i R, composed of the 1307 right eye images from 139 subjects.

In our tests, we considered as ground truth the masks manually segmented by Operator A, as described in Hofbauer et al. (2014).

4.1.5. DB IITD

is composed of samples acquired using commercial iris scanners in controlled conditions. It a is subset of "IIT Delhi Iris Database Version 1.0" database (Kumar and Passi (2010)).

In this work we define DB IITD as a set of 1.120 samples corresponding to the left and right eyes of 224 subjects, for which manually segmented masks are publicly available, as described in Hofbauer et al. (2014). The images correspond to left and right eyes and have a size of 320 × 240 pixels.

In our tests, we considered as ground truth the masks manually segmented by Operator A, as described in Hofbauer et al. (2014).

4.1.6. DB Notredame

is composed of samples acquired using commercial iris scanners in controlled conditions. It a is subset of "ND-Iris-405" database (Phillips et al. (2010)).

In this work we define DB Notredame as a set of 2.640 samples corresponding to the left and right eyes of 260 subjects, for which manually segmented masks are publicly available, as described in Hofbauer et al. (2014). The images correspond to left and right eyes and have a size of 640×480 pixels.

In our tests, we considered as ground truth the masks manually segmented by Operator A, as described in Hofbauer et al. (2014).

4.2. Performance evaluation and figures of merit

To evaluate the accuracy and the generality of our segmentation method to improve the final recognition accuracy of iris recognition systems in non-ideal conditions, we used six publicly available recognition schemes for feature extraction and matching. The first schema consists of the feature extraction and matching algorithms based on log-Gabor features (LG) and described in Masek and Kovesi (2003). To reduce the computation time required for each test, we implemented Masek's matching algorithm in C language, while we used the original implementation of the feature extractor. The other recognition schemes are implemented in the USIT software version 2.2, described in Rathgeb et al. (2016), and are the following ones: Complex Gabor (CG), described in Daugman (2002); Quadratic Spline Wavelet (QSW), described in Ma et al. (2004), Cumulative sums of gray scale blocks (KO), described in Ko et al.; and Local intensity variations (CR), described in Rathgeb and Uhl (2010). The figures of merit used were: Receiver Operating Characteristic (ROC) curves, described in Jain et al. (2007); Equal Error Rate (EER), as detailed in Maio et al. (2002); FAR_{100} (False Rejection Rate - FRR - at False Acceptance Rate - FAR - of 1.00%); FAR_{1000} (FRR at FAR of 0.10%).

Another test consisted of evaluating the pixel-wise segmentation accuracy. For this test, we used publicly available segmentation masks describing the iris boundaries as closed curves and the upper and lower occlusions as polynomials. We choose these masks since they have been used in feature extraction and matching algorithms, as described in Rathgeb et al. (2016). We used the figures of merit adopted for the competition NICE.I. In particular, the classification error rate (E^1) is computed as the proportion of correspondent disagreeing pixels (through the logical exclusive-or operator) between each computed segmentation mask and the corresponding manually segment mask. This metric is computed as: $E^1 = \frac{1}{n}\sum_i \frac{1}{c \times r}\sum_{c'}\sum_{r'} O_i(c', r') \otimes C_i(c', r')$ where, n is the number of images, $O_i(c', r')$ and $C_i(c', r')$ are, respectively, pixels of the computed mask and the real mask of image i, and $\otimes$ represents the XOR operation. The second metric (E2) aims to compensate the disproportion between the False Positive Rate (FPR) and False Negative Rate (FNR) of the pixelwise classification. This metric is computed as: $E^2 = (1/n) \times 0.5 \times \mathrm{FPR}_i + 0.5 \times \mathrm{FNR}_i$.

For each dataset, we computed the recognition accuracy achieved by different segmentation tools. In particular we considered three segmentation algorithms included in USIT version 2.2: the weighted adaptive Hough and ellipsopolar transform (Wahet), presented in Wild et al. (2015); the contrast-adjusted Hough transform (Caht) presented in Rathgeb et al. (2013); the iterative Fourier-series push pull (Ifpp), presented in Daugman (2007). Furthermore, we computed the performance of a segmentation technique based on the Total Variation Model (Tvm), presented in Zhao and Kumar (2015); and of a fast segmentation algorithm for non-ideal images (Fsa), presented in Gangwar et al. (2016). We also compared the pixel-wise segmentation accuracy achieved by the proposed method with that of the three configurations of the approach based on deep learning presented in Jalilian and Uhl (2017) (Dl Original, Dl Basic, and Dl Bayesian-Basic) where possible, in particular with datasets DB UBIRIS v2, DB CASIA v4i, DB IIT, DB Notredame.

4.3. Segmentation accuracy in non-ideal conditions

Table 4 summarizes the obtained results for the non-ideal image datasets DB QFIRE, DB WVU, and DB UBIRIS v2. For space constraints, we do not report the results achieved using every evaluated recognition schema. Table 4 reports the accuracy for the recognition schemes LG, CG, and QSW. We report the results of the first two recognition schemes since they are widely used in the literature, and the results of QSW because it achieved the best recognition accuracy. For DB QFIRE, the reported results refer to 35,090 genuine identity comparisons and 6,711,916 impostor identity comparisons. For DB WVU, the reported results are based on 20,920 genuine identity comparisons and 9,579,782 impostor identity comparisons. For DB UBIRIS v2, the reported results refer to 54,000 genuine identity comparisons and 5,006,250 impostor identity comparisons. Table 4 shows that PS-RANSAC achieved the best accuracy with respect to compared methods.

In the following, we examine the results obtained for each dataset and compare the performance of PS-RANSAC with additional results reported in the literature for the best performing state-of-the-art techniques.

4.3.1. DB QFIRE

As reported in Table 4, PS-RANSAC achieved the best accuracy with respect to the compared segmentation methods for the recognition schemes LG and CG, which use Gabor-based features. PS-RANSAC achieved an EER of 5.98% with LG and 9.20% with CG. For the recognition schema QSW, PS-RANSAC reached the second place, with EER 5.52%.

Furthermore, we applied the commercial-of-the-shelf segmentation method described in NEUROtechnology, which discarded the 3.9% of the samples for insufficient quality and achieved an EER of 7.53% for the remaining images. The achieved performance shows that the proposed segmentation method can be applied to images acquired at different distances from the eye, in heterogeneous illumination conditions with satisfactory accuracy for different feature extractors and matchers.

We also compared the performance of the proposed PS-RANSAC method with that of other methods reported in the literature for external boundary segmentation using the feature extraction and matching algorithms described in Masek

Table 4. Comparison of segmentation accuracy for datasets of iris images acquired in non-ideal conditions

Segmentation method	DB QFIRE					DB WVU					DB UBIRIS v2				
	Segmentation		Verification - EER (%)			Segmentation		Verification - EER (%)			Segmentation		Verification - EER (%)		
	E1	E2	LG	CG	QSW	E1	E2	LG	CG	QSW	E1	E2	LG	CG	QSW
Dl Original†	(∼)	(∼)	(–)	(–)	(–)	(∼)	(∼)	(–)	(–)	(–)	0.0305	0.0898	(–)	(–)	(–)
Dl Basic†	(∼)	(∼)	(–)	(–)	(–)	(∼)	(∼)	(–)	(–)	(–)	0.0262	0.0687	(–)	(–)	(–)
Dl Bayesian-Basic†	(∼)	(∼)	(–)	(–)	(–)	(∼)	(∼)	(–)	(–)	(–)	0.0187	0.0675	(–)	(–)	(–)
Wahet	(∼)	(∼)	15.49	17.24	15.83	(∼)	(∼)	4.75	11.55	6.97	0.2621	0.4783	(+)	(+)	(+)
Ifpp	(∼)	(∼)	17.69	19.81	18.80	(∼)	(∼)	10.29	14.82	13.70	0.2282	0.3789	(+)	(+)	(+)
Caht	(∼)	(∼)	(+)	(+)	(+)	(∼)	(∼)	14.70	19.19	12.21	0.1088	0.4525	(+)	(+)	(+)
Fsa	(∼)	(∼)	7.44	19.24	**4.96**	(∼)	(∼)	4.91	15.57	6.67	0.1720	0.4310	(+)	(+)	(+)
Tvm	(∼)	(∼)	20.80	25.04	23.82	(∼)	(∼)	(+)	(+)	(+)	0.0211	0.1172	(+)	(+)	(+)
MSR + PS-RANSAC	(∼)	(∼)	**5.98**	**9.20**	5.52	(∼)	(∼)	**4.34**	**10.55**	**5.27**	**0.0165**	**0.0588**	(+)	(+)	(+)

Notes: †result reported in Jalilian and Uhl (2017) and regarding machine learning method trained and tested using a 10-fold cross-validation procedure; (∼) result not computed because segmentation masks created by human operators are not publicly available; (–) result not computed because the segmentation algorithm is not publicly available ; (+) EER > 30%. The error metrics E1 and E2 have been computed using the publicly available segmentation masks described in Hofbauer et al. (2014) as ground truth.

and Kovesi (2003). The algorithms used for steps A (noise reduction), B (internal boundary segmentation) and C (illumination compensation based on MSR) of our segmentation method were identical in each test. To compare the performances of the evaluated methods, we used the same feature extraction and matching techniques and substituted only step D (external boundary segmentation) of our segmentation method with other well-known techniques. In detail, step D (external boundary segmentation) was performed using the following techniques: RANSAC for circle fitting, the algorithm based on Discrete Fourier Series analysis described in Daugman (2007), and the algorithm designed for noisy iris images presented in Donida Labati and Scotti (2010). Fig. 10 (a) shows the obtained ROC curves. PS-RANSAC demonstrated better performance compared with the other techniques. PS-RANSAC achieved the best accuracy, with EER of 5.98% and and FAR_{1000} = 13.39%.

The achieved performance show that the proposed segmentation method can be applied to images acquired at different distances from the eye and in heterogeneous illumination conditions with satisfactory accuracy for different recognition schemes.

4.3.2. DB WVU

As reported in Table 4, PS-RANSAC achieved the best accuracy with respect to the compared publicly available methods for DB WVU. The best result is an EER of EER = 4.34%, achieved using the recognition schema LG.

To the best of our knowledge, the only previous paper that has evaluated the accuracy of an iris segmentation method for DB WVU in terms of its contribution to the overall biometric recognition accuracy is Shah and Ross (2009), which presented a robust segmentation approach based on Geodesic Active Contours. It achieved EER of 12.03% for the left eyes and 14.19% for the right eyes. Other iris segmentation methods reported in the literature have been evaluated using different figures of merit. The authors of Zuo and Schmid (2010) and Zuo et al. (2006) reported segmentation success rates of 97.92% and 95.84%, respectively. However, this figure of merit is subjective because the segmentation results were visually classified as either correct or incorrect. Therefore, the performance of the proposed method cannot be directly compared with the performances of these algorithms. Other segmentation techniques cannot be directly compared with the proposed approach because they have only been tested using subsets of DB WVU. For example, the technique presented in Roy et al. (2010) was validated using a subset of 800 images, and that described in Pundlik et al. (2008) was tested using 60 images over the 3099 composing the complete dataset.

Furthermore, we compared the performance achieved using PS-RANSAC with the results reported in Proenca and Neves (2017). These results have been obtained by applying a coarse-to-fine segmentation strategy based on geodesic active contours and recent recognition methods specifically designed to deal with non-ideal samples, which are based on computational intelligence techniques. It emerged that, although using recognition methods not optimized for this dataset of non-ideal samples, PS-RANSAC allowed to achieve a recognition accuracy close to the best performing biometric recognition system described in Proenca and Neves (2017). Specifically, the EER values achieved by PS-RANSAC in conjunction with the matching method presented in Masek and Kovesi (2003) and by the biometric system described in Proenca and Neves (2017) are 4.3% and 4.2%, respectively. Moreover, PS-RANSAC permitted to achieve better recognition performance than the recent matching methods presented in Yang et al. (2015) and Sun and Tan (2009), which achieved EER values equal to 9.50% and 13.37%, respectively. We think that this result is encouraging and proves the positive contribution of PS-RANSAC can provide to current biometric recognition systems, also without using machine learning approaches.

Furthermore, we applied the commercial-of-the-shelf segmentation method described in NEUROtechnology, which discarded the 0.1% of the samples for insufficient quality and achieved an EER of 0.9% for the remaining images. We think that this method obtained a better recognition accuracy with respect to the state of the art thanks to a robust matcher. Unfortunately, the SDK does not allow to evaluate the segmentation accuracy or use the feature extraction algorithm in conjunction with arbitrary segmentation methods.

Similarly to the tests performed using DB QFIRE, we compared the performance of the proposed PS-RANSAC method with the performances of other methods reported in the literature for external boundary segmentation. Fig. 10 (b) shows the obtained ROC curves. Also in this case, PS-RANSAC achieved

the best accuracy, with EER = 4.34% and FAR_{1000} = 12.38%.

The obtained results show that the proposed method is robust to samples acquired using iris scanners but affected by strong nonidealities, allowing different recognition schemes to achieve remarkable accuracy.

4.3.3. DB UBIRIS v2

For DB UBIRIS v2, Table 4 shows that PS-RANSAC achieved better results than the compared methods, also based on machine learning strategies. In our opinion, this result is particularly relevant, showing the robustness of our method in selecting the region of interest for real biometric recognition applications. The obtained results prove that the proposed segmentation method can be successfully applied directly to the red channel of color-based images. However, it should be taken into account to properly tune the pupil detection algorithm of the proposed method since the iris-pupil contrast can be low for dark eyes, thus introducing possible segmentation errors. Furthermore, the considered feature extraction algorithms and matching methods are designed for images acquired using infrared illuminators and obtain unsatisfactory performance for images acquired in natural light illumination (EER > 30%). As discussed in Bowyer (2012), biometric recognition systems based on iris images acquired in natural light conditions require dedicate feature extraction and matching algorithms.

We also evaluated the pixel-wise segmentation accuracy of the proposed method on the subset of 500 iris images of the second version of UBIRIS used as test dataset for the NICE.I competition, adopting the manually segmented masks used for this competition as ground truth, as described in Proenca and Alexandre (2007). In the following, we refer to this set of images as DB NICE 1. The manually segmented masks of DB NICE 1 present finer level of details with respect to the ones from DB UBIRIS v2, since they consider reflections and small occlusions due to hairs, glasses and single eyelashes. The proposed segmentation method achieved E1 = 0.021. Manually segmenting the pupil region and applying PS-RANSAC to segment the external iris boundary, we achieved E1 = 0.018. Our previously proposed method was one of the finalists of the NICE.I competition, achieving E1 = 0.030 for DB NICE 1 by using algorithms for segmenting small occlusions and reflections. More recent methods designed to detect reflections and small occlusions can achieve better results. For example, Tvm achieved E1 = 0.012. Novel methods based on deep learning, as the ones described in Arsalan et al. (2017), further decreased the segmentation error for this subset of images. However, these methods require a time-consuming training step for being used in other application scenarios. On the contrary, the proposed method can be applied to a wide range of heterogeneous scenarios without needing any training step.

4.4. Segmentation accuracy in ideal conditions

Although the proposed method is designed for non-ideal scenarios, we evaluated its accuracy also for samples acquired using commercial iris scanners in ideal conditions (DB CASIA v4i, DB IITD, and DB Notredame). We used the same protocol adopted for databases of images acquired in non-ideal scenarios. Table 5 summarizes the obtained results. For completeness,

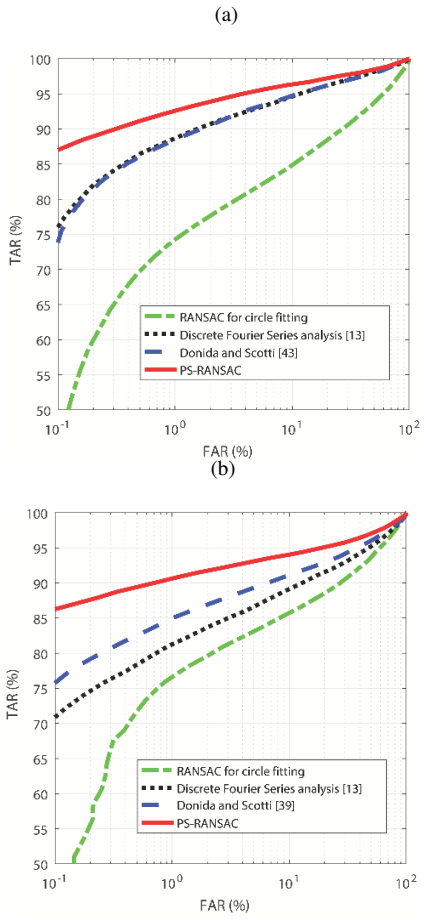

Fig. 10. ROC curves obtained using the proposed method with different algorithms for performing the external boundary segmentation (step D) for: (a) DB WVU, and (b) DB QFIRE. The evaluated algorithms are: RANSAC for circle fitting, the algorithm based on Discrete Fourier Series analysis described in Daugman (2007), the method designed for noisy iris images presented in Donida Labati and Scotti (2010), and the proposed PS-RANSAC algorithm.

we computed also the segmentation accuracy of PS-RANSAC for DB CASIA v4i, achieving E^1 = 0.03760 and E^2 = 0.04066, which are close to the values obtained for DB CASIA v4i R (E^1 = 0.0392 and E^2 = .0436). The pixel-wise segmentation accuracy as well as the verification accuracy achieved using PS-RANSAC are comparable to ones of segmentation methods specifically designed for samples acquired using iris scanners in controlled conditions and ones of the machine learning approaches trained separately for each dataset.

The obtained results show that although the proposed segmentation method has been designed for samples acquired in non-ideal conditions, it can achieve an accuracy comparable to trained methods based on deep learning techniques.

4.5. Impact of illumination compensation techniques on the segmentation accuracy

We compared the performance achieved using our segmentation algorithm in combination with various illumination compensation techniques (Section II-B) for samples acquired in particularly challenging conditions (DB QFIRE, DB WVU, and DB UBIRIS v2). The algorithms used for the steps A (noise

Table 5. Comparison of segmentation accuracy for datasets of iris images acquired in ideal conditions

Segmentation method	DB CASIA v4i R					DB IITD					DB Notredame				
	Segmentation		Verification - EER (%)			Segmentation		Verification - EER (%)			Segmentation		Verification - EER (%)		
	E1	E2	LG	CG	QSW	E1	E2	LG	CG	QSW	E1	E2	LG	CG	QSW
Dl Original†	0.0561	0.0588	(–)	(–)	(–)	0.0561	0.0588	(–)	(–)	(–)	0.0213	0.0424	(–)	(–)	(–)
Dl Basic†	0.0448	0.0438	(–)	(–)	(–)	0.0539	0.0594	(–)	(–)	(–)	**0.0107**	**0.0269**	(–)	(–)	(–)
Dl Bayesian-Basic†	0.0391	0.0407	(–)	(–)	(–)	0.0682	0.0701	(–)	(–)	(–)	0.0095	0.0282	(–)	(–)	(–)
Wahet	0.0615	0.0582	2.31	6.65	5.49	0.0978	0.0951	5.32	**13.32**	8.33	0.0266	0.0429	9.39	**13.76**	9.58
Ifpp	0.0771	0.0848	8.42	3.99	5.46	0.0911	0.0831	3.80	16.90	16.55	0.0285	0.0493	12.54	17.04	19.39
Caht	0.0291	**0.0372**	**1.17**	**1.72**	1.44	0.0494	0.0695	2.18	16.93	9.86	0.0232	0.0841	10.41	17.92	10.24
Fsa	**0.0275**	0.0420	1.54	2.26	**0.46**	**0.0330**	**0.0364**	**0.70**	18.60	**4.94**	0.0118	0.0426	**5.47**	18.57	**4.94**
Tvm	0.2542	0.3956	(+)	(+)	(+)	0.3422	0.5048	(+)	(+)	(+)	0.0879	0.3683	(+)	(+)	(+)
MSR + PS-RANSAC	0.0392	0.0436	3.33	4.69	3.58	0.0780	0.0848	4.02	13.72	7.65	0.0163	0.0334	7.98	14.49	8.98

Notes: †result reported in Jalilian and Uhl (2017) and regarding machine learning method trained and tested using a 10-fold cross-validation procedure; (–) result not computed because the segmentation algorithm is not publicly available ; (+) EER > 30%. The error metrics E1 and E2 have been computed using the publicly available segmentation masks described in Hofbauer et al. (2014) as ground truth.

reduction), B (internal boundary segmentation) and D (external boundary segmentation) of our segmentation method were identical in each test, but we tested the use of different algorithms for step C (illumination compensation).

We performed a broad study of illumination compensation techniques, which included: algorithms based on the histogram equalization, algorithms based on the analysis of the histogram distribution, algorithms based on the local histogram analysis, SSR, MSR, DCT, TT and SQI. The first three classes of techniques yielded satisfactory results only for iris images in which the iris presented stable characteristics, such as similar iris diameters and acquisition conditions. In fact, these techniques require the tuning of one or more parameters that are expected to have the same value for each iris image. However, the considered iris images exhibited significant differences in iris diameter (from approximately 110 pixels to more than 300 pixels). Therefore, the optimal parameters for these techniques could differ considerably for different iris images. For this reason, we do not report the results achieved for these algorithms. SSR was tuned by using different Gaussian filters to estimate the luminance L (Gaussian filters of 8×8, 16×16, 32×32, 64×64, 128×128, and 256×256 pixels). MSR was tuned by using all possible combinations of two of the filters used for SSR. DCT was tuned by using $5, 10, 15, 20, 25, 30$ and 35 components. TT was tuned by using the gamma intensity correction parameters $0.05, 0.1, 0.2, 0.5$, and 1. SQI was tuned by using filters of size 9×9, 17×17, 33×33, 65×65, and 129×129 pixels.

For DB UBIRIS v2 we performed the comparison in terms of E^1. For DB WVU and DB QFIRE the performance were compared in terms of recognition accuracy. In the last case, we used the same feature extraction and matching techniques. We computed the results applying the feature extraction and matching algorithms LG since it is widely used in the literature and previous tests showed that the performance of the considered feature extraction and matching methods decrease in a similar way in presence of segmentation errors. The experiments revealed that illumination compensation algorithms enhanced the segmentation accuracy and, thus, the ultimate performance of the iris recognition system. The methods that yielded the best results were SSR, MSR and DCT.

Table 6 presents the results of the illumination compensation study for DB UBIRIS v2, expressed in term of E^1. The parameters of the best configurations of the illumination compensation methods are the following: Gaussian filters of 128×128 for SSR, kernels of size 64×64 and 128×128 pixels for MSR, 10 coefficients for DCT, gamma intensity of 0.2 for TT, and kernel of 17×17 pixels for SQI. In general, all the tested methods helped to significantly improve the segmentation accuracy when their parameters were accurately selected. Our method obtained the best segmentation accuracy with SSR and MSR. Since the main nonidealities due to poor illumination conditions that are present in the images of DB UBIRIS v2 are smooth shadows, we think that SSR and MSR achieved the best performance caused by their capability of reducing problems due to smooth illumination changes. DCT achieved similar performance. TT was also capable of improving the results of our segmentation algorithm, but not as much as in the cases of SSR and MSR. We think that the main cause for this might be strong artificial gray level edges introduced in the DoG convolution, because it was not possible to mask irrelevant regions, such as skin or eyebrows. SQI provided also good results, although they were not as impressive as with SSR and MSR. Furthermore, SQI was less robust to parameter changes and introduced some artifacts in the iris images.

Table 6. Effects of different illumination compensation techniques on the pixel-wise segmentation accuracy of the proposed PS-RANSAC method evaluated on DB UBIRIS v2.

Illumination Compensation	Results (E^1)
PS-RANSAC	0.0217
SSR + PS-RANSAC	**0.0165**
MSR + PS-RANSAC	**0.0165**
DCT + PS-RANSAC	0.0167
TT + PS-RANSAC	0.0191
SQI + PS-RANSAC	0.0176

We report the results obtained by the three illumination compensation algorithms that achieved the best performance for DB UBIRIS v2 (SSR, MSR, and DCT) on the segmentation accuracy of the proposed method by evaluating the recognition performance for DB WVU and DB QFIRE. The best results for SSR were obtained using Gaussian filters of 256×256 pixels. For DB WVU, the optimal MSR configuration consisted of two Gaussian filters of 32×32 pixels and 128×128 pixels, while the optimal DCT configuration consisted of 15 coefficients. For DB QFIRE, the optimal MSR configuration consisted of two

Table 7. Effects of different illumination compensation techniques on the recognition accuracy of the proposed PS-RANSAC method evaluated on DB WVU and DB QFIRE.

Database	Illumination Compensation	EER (%)	FAR_{100}(%)	FAR_{1000}(%)
DB WVU	PS-RANSAC	4.63%	7.79%	12.97%
DB WVU	SSR + PS-RANSAC	4.57%	7.43%	12.51%
DB WVU	**MSR + PS-RANSAC**	**4.34%**	**7.35%**	**12.38%**
DB WVU	DCT + PS-RANSAC	4.44%	8.06%	13.67%
DB QFIRE	PS-RANSAC	6.61%	10.30%	14.96%
DB QFIRE	SSR + PS-RANSAC	6.31%	9.75%	13.70%
DB QFIRE	**MSR + PS-RANSAC**	**5.98%**	**9.50%**	**13.39%**
DB QFIRE	DCT + PS-RANSAC	6.21%	9.50%	13.97%

Gaussian filters of 16×16 pixels and 64×64 pixels, while the optimal DCT configuration consisted of 5 coefficients. Table 7 present the results obtained for the optimal configurations of the evaluated illumination compensation algorithms. The table shows that the use of an illumination compensation algorithm improved the recognition performance of our proposed PS-RANSAC segmentation method for non-ideal images acquired with infrared illumination using traditional iris scanners as well as non-ideal images acquired at different distances using digital cameras. In this context, MSR produced images that were less affected by blur compared with those obtained using SSR and DCT, and therefore yielded greater improvements in segmentation performance and recognition accuracy compared with SSR and DCT. The illumination compensation methods contributed more strongly to the overall segmentation accuracy for DB QFIRE than for DB WVU. This finding can be attributed to the fact that the samples in the first dataset were deliberately captured under poor illumination conditions and exhibit lower iris-sclera contrast. Nevertheless, the application of MSR did result in a slight increase in segmentation accuracy for DB WVU, likely reducing the disadvantageous effects of overexposure and underexposure of local regions in the images caused by incorrect positioning of the subjects with respect to the commercial iris scanner. Moreover, the obtained results show that our algorithm for the segmentation of the external iris boundary (PS-RANSAC) also achieved satisfactory results for the original low-contrast images.

Fig. 11 shows examples of pairs of samples and the corresponding match scores (m_s) obtained by using PS-RANSAC and the recognition schema LG. The images have been segmented without applying any illumination compensation technique and by applying MSR in its optimal configuration. MSR can mitigate problems caused by poor illumination conditions, thereby improving the segmentation accuracy and the overall recognition error of the biometric system.

The primary focus of this paper is on iris segmentation. However, we also report the results of tests on the use of illumination compensation techniques to improve the visibility of distinctive iris characteristics prior to the feature extraction step of the biometric recognition process for samples affected by important nonidealities and acquired using infrared illumination. We used the segmentation masks obtained using our segmentation method in its optimal configuration (MSR + PS-RANSAC) and then applied SSR, MSR, and DCT in various configurations both to the iris image I (modality A) and to the normalized image obtained by applying the Rubber Sheet Model (as described in Daugman (2002)) to I (modality B). In the tests of modality A, we tuned the SSR algorithm by using different Gaussian filters to estimate the luminance L (Gaussian filters of 8×8, 16×16, 32×32, 64×64, 128×128, and 256×256 pixels). Similarly, the MSR algorithm was tuned by using all possible combinations of two of the filters used for SSR. We also used DCT with 5, 10, 15, 20, 25, 30, and 35 coefficients. In the tests of modality B, we again tuned the SSR algorithm by using different Gaussian filters to estimate the luminance L (in this case, Gaussian filters of 4×4, 8×8, 12×12, 16×16, and 20×20 pixels), tuned the MSR algorithm by using all possible combinations of two of the filters used for SSR, and applied DCT with 4, 6, 8, and 10 coefficients. We performed these tests by using the feature extraction and matching algorithms LG.

Modality A with an MSR configuration consisting of Gaussian filters of 8×8 and 16×16 pixels yielded the best results for both DB WVU and DB QFIRE. For DB WVU, the application of illumination compensation reduced the FAR_{1000} from 12.38% to 10.69%, with EER of 4.91%. For DB QFIRE, the application of illumination compensation did not increase the recognition accuracy. Modality B did not improve the performance of the biometric system.

The results suggest that methods based on the Retinex model can reduce the hindering effects of poor illumination conditions on feature extraction and matching in iris recognition systems. However, more detailed studies are needed to improve the performance of iris recognition for images acquired at a distance. This topic should be the subject of future work.

4.6. Computational time

We executed the tests using a PC with 3.7 GHz Intel (R) Xeon (R) E5-1620 v2 CPU, RAM 16 GB. The operating system was Windows 10 professional 64 bit. We implemented all the algorithms using Matlab 2016a. The mean computational time needed to segment an iris image was around 0.21 seconds, of which 0.10 was needed by PS-RANSAC. We think that the computational cost of our method is acceptable since Matlab is a prototype-oriented and non-optimized environment. We expect that the use of compiled languages, such as C/C++, can further reduce the processing time.

5. Discussion

To evaluate the accuracy of the proposed segmentation method, we performed identity verification tests using datasets acquired in heterogeneous conditions: DB QFIRE, DB WVU, DB UBIRIS v2, DB CASIA v4i, DB IITD, and DB Notredame. For datasets for which segmentation masks created by human operators are available, we also evaluated the pixelwise segmentation accuracy. In all the cases, we compared the obtained results with other techniques in the literature and publicly available software. For samples acquired in non-ideal conditions acquired using infrared illuminators, the proposed method achieved the best identity verification accuracy with respect to the compared techniques using a feature extractor based on log-Gabor filters, with EER of 4.34% for DB WVU and

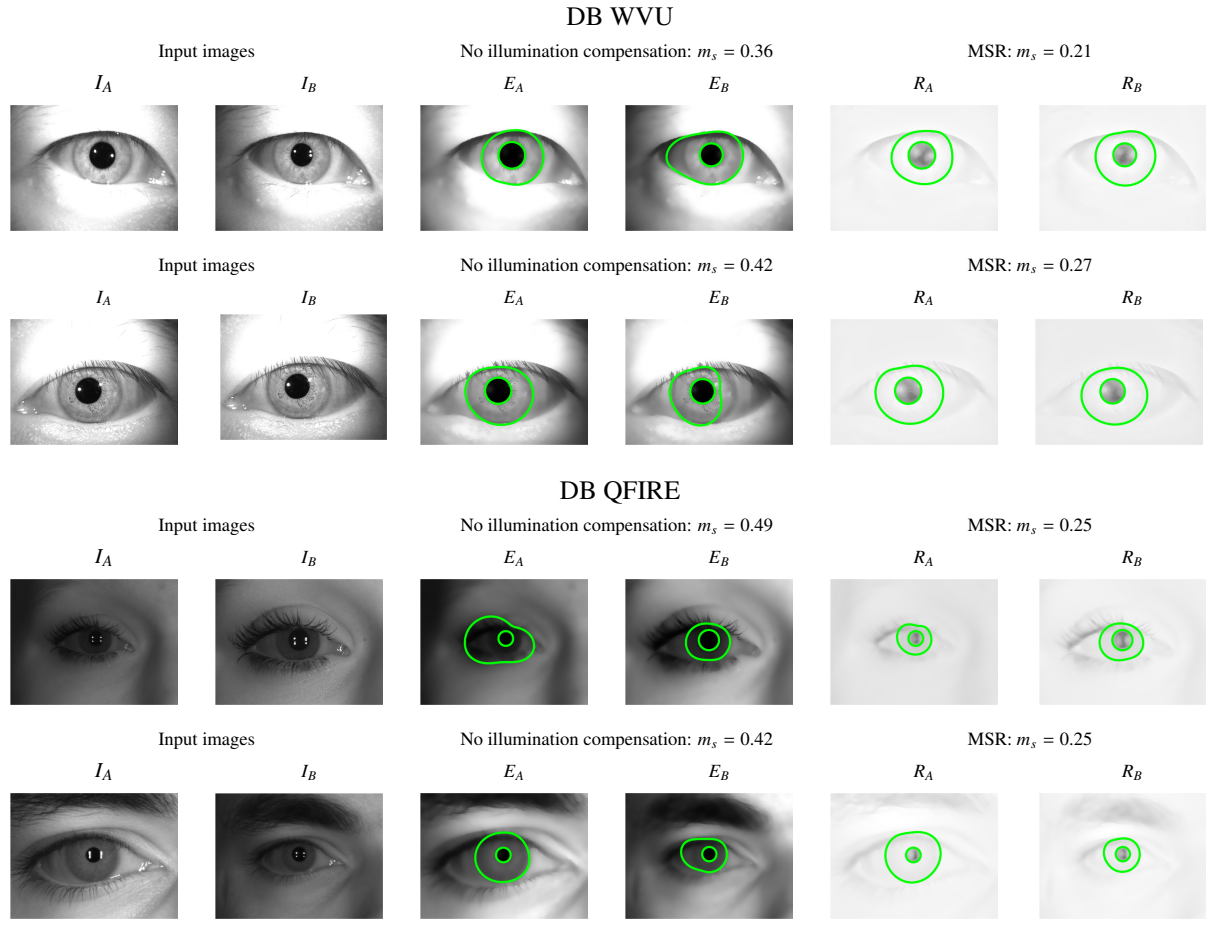

Fig. 11. Examples of pairs of samples and the corresponding match scores (m_s) obtained by using PS-RANSAC and the recognition schema LG. The images have been segmented without applying any illumination compensation technique and by applying MSR in its optimal configuration. MSR mitigates problems caused by poor illumination conditions, thereby improving the segmentation accuracy and the overall recognition error of the biometric system.

5.98% for DB QFIRE. For non-ideal images acquired in visible light illumination, PS-RANSAC achieved the best pixelwise classification accuracy, with a classification error rate of 0.0165 for the 2250 iris images of DB UBIRIS v2. In case of images acquired using iris scanners in cooperative scenarios, the proposed method achieved pixelwise classification accuracy and identity verification accuracy comparable to recent approaches based on deep learning and algorithms specifically designed for this category of samples. Specifically, PS-RANSAC achieved a pixel-wise classification error E1 of 0.0392 for DB CASIA v4i, 0.0780 for DB IITD, and 0.0163 for DB Notredame.

Furthermore, tests performed using various illumination compensation techniques showed that the application of these algorithms can improve segmentation performance. Among all the tested algorithms, MSR was the one that provided the best improvement in segmentation accuracy. An analysis of the use of illumination compensation techniques to improve performance in the feature extraction step of the biometric recognition process also indicated an encouraging improvement in matching performance.

6. Conclusion

This paper presented a novel iris segmentation method, referred to as Polar Spline RANSAC or PS-RANSAC, designed for application to samples affected by strong non-idealities and acquired under poor illumination conditions. The presented method can achieve competitive performance for different types of feature extraction and matching techniques, and can deal with multiple scenarios: iris images acquired using traditional near infrared iris sensors; infrared iris images acquired at a great distance; and iris images acquired in the visible spectrum. Moreover, the paper analyzed the application of various illumination compensation techniques in conjunction with PS-RANSAC to further improve performance. We evaluated the accuracy of the proposed iris segmentation method using six challenging image datasets acquired in heterogeneous conditions, achieving better or comparable accuracy in every scenario. The achieved results show that PS-RANSAC can be applied with competitive accuracy for a wider set of non-ideal acquisition conditions with respect to the considered state-of-the-art methods, without needing any preliminary training step. Furthermore, we experimentally demonstrated that illumination compensation techniques based on the Retinex model can increase the segmentation and identity verification accuracy of iris recognition systems.

Future work should address novel illumination compensation techniques designed to improve feature extraction for iris images. Particular attention should be on methods designed for

images acquired at a large distance between the subject and the camera.

7. Acknowledgements

R. Donida Labati, E. Muñoz, V. Piuri, and F. Scotti were supportedin part by the Italian Ministry of Research within PRIN 2015 projectCOSMOS (201548C5NT). A. Ross was supported in part by the NationalScience Foundation under Grant Number 1618518.

8. Appendix. Parameters of the proposed method

The parameters of the proposed algorithms were empirically estimated based on the image datasets considered in this study.

The threshold value used to search for specular reflections was set to $p_r = 95\%$. The parameters of the bilateral filter were set to $N_q = 22$ pixels, $\sigma_s = 16$ and $\sigma_r = 0.1$, $\sigma_s = 2$. The intensity values used to estimate the pupil shape were $T = [10, 15, \ldots, 25]$ for DB QFIRE. The estimation of the points representing the external iris boundary was performed using an r_{min} value equal to 15 pixels plus the pupil radius and $N_m = 16$ pixels. PS-RANSAC was applied using $N = 6$, while the proportion "hypothetical inliers" of the points in the input set X n_p was set to 0.9.

For DB WVU, the only parameter different from the previously described configuration is the one describing the intensity values considered for segmenting the pupil region, which have values $T = [20, 25, \ldots, 65]$.

Although images acquired in visible light and infrared illumination present strongly different characteristics, many parameters used for DB UBIRIS v2 are the same as the ones used for DB QFIRE. The other parameters are $N_q = 10$ pixels, $\sigma_s = 2$ $\sigma_r = 0.1$, $T = [2, 4, \ldots, 106]$, and $n_p = 1$.

As in the case of DB WVU, for the other datasets of images acquired in near infrared illumination, the only parameters with different values with respect to the ones used for DB QFIRE are the ones used to segment the pupil. Specifically: $T = [20, 10, \ldots, 80]$ for DB CASIA v4i, $T = [10, 5, 15]$ for DB IITD, and $T = [3, 3, \ldots, 15]$ for DB Notredame.

We tested the robustness of the proposed segmentation approach by evaluating the accuracy with respect to a wide range of different values of the parameters obtaining satisfactory results. As an example, when we evaluated the performance of PS-RANSAC on DB WVU and DB QFIRE with $N = [3, 4, \ldots, 10]$ and $n_p = [0.5, 0.6, \ldots, 1.0]$, we obtained a maximum decrease in the EER of approximately 1%. Table 8 presents the variation of E^1 for DB UBIRIS v2 with respect to the most important parameter of PS-RANSAC, N. This table shows that the method is robust to different values of its parameters, providing only small performance variations for each of the considered configurations.

Table 8. Variation of E^1 for DB UBIRIS v2 for different values of the parameter N.

N	4	6	8	10
E^1	0.0175	0.0165	0.0168	0.0171

References

Abdullah, M.A.M., Dlay, S.S., Woo, W.L., Chambers, J.A., 2017. Robust iris segmentation method based on a new active contour force with a noncircular normalization. IEEE Trans. on Systems, Man, and Cybernetics: Systems 47, 3128–3141.

Aligholizadeh, M.J., Javadi, S., Sabbaghi-Nadooshan, R., Kangarloo, K., 2011. An effective method for eyelashes segmentation using wavelet transform, in: Proc. Int. Conf. Biometrics and Kansei Eng., pp. 185–188.

Alonso-Fernandez, F., Farrugia, R.A., Bigun, J., 2015. Reconstruction of smartphone images for low resolution iris recognition, in: IEEE Int. Workshop Inf. Forensics and Security), pp. 1–6.

Arsalan, M., Hong, H.G., Naqvi, R.A., Lee, M.B., Kim, M.C., Kim, D.S., Kim, C.S., Park, K.R., 2017. Deep learning-based iris segmentation for iris recognition in visible light environment. Symmetry 9.

Arsalan, M., Naqvi, R.A., Kim, D.S., Nguyen, P.H., Owais, M., Park, K.R., 2018. Irisdensenet: Robust iris segmentation using densely connected fully convolutional networks in the images by visible light and near-infrared light camera sensors. Sensors 18.

Bazrafkan, S., Thavalengal, S., Corcoran, P., 2018. An end to end deep neural network for iris segmentation in unconstrained scenarios. Neural Networks 106, 79 – 95.

Bertalmio, M., Sapiro, G., Caselles, V., Ballester, C., 2000. Image inpainting, in: Proc. 27th Annu. Conf. Comput. Graph. and Interactive Techn., pp. 417–424.

Boddeti, N., Kumar, B.V.K.., 2008. Extended depth of field iris recognition with correlation filters, in: Proc. 2nd IEEE Int. Conf. Biometrics: Theory, Appl. and Syst., pp. 1–8.

Bowyer, K.W., 2012. The results of the nice.ii iris biometrics competition. Pattern Recogn. Lett. 33, 965–969.

Broussard, R., Kennell, L., Soldan, D., Ives, R., 2007. Using artificial neural networks and feature saliency techniques for improved iris segmentation, in: Int. Joint Conf. Neural Networks, pp. 1283–1288.

Chen, W., Er, M.J., Wu, S., 2006. Illumination compensation and normalization for robust face recognition using discrete cosine transform in logarithm domain. IEEE Trans. on Systems, Man, and Cybernetics, Part B (Cybernetics) 36, 458–466.

ho Cho, D., Park, K.R., Rhee, D.W., Kim, Y., Yang, J., 2006. Pupil and iris localization for iris recognition in mobile phones, in: Proc. ACIS Int. Conf. on Software Engineering, Artificial Int., Networking, and Parallel/Distr.Comp., pp. 197–201.

Choi, S., Kim, T., Yu, W., 2009. Performance evaluation of ransac family, in: Proc. Brit. Mach. Vision Conf., pp. 81.1–81.12.

Chou, C.T., Shih, S.W., Chen, W.S., Cheng, V., Chen, D.Y., 2010. Non-orthogonal view iris recognition system. IEEE Trans. Circuits Syst. Video Technol. 20, 417–430.

Crihalmeanu, S., Ross, A., Schuckers, S., Hornak, L., 2007. A Protocol for Multibiometric Data Acquisition, Storage and Dissemination. Technical Report. Lane Depart. Comput. Sci. and Elect. Eng., West Virginia University.

Daugman, J., 2002. How iris recognition works. IEEE Trans. Circuits Syst. Video Technol. 14, 21–30.

Daugman, J., 2007. New methods in iris recognition. IEEE Trans. Syst., Man, Cybern., B, Cybern. 37, 1167–1175.

Donida Labati, R., Genovese, A., Piuri, V., Scotti, F., 2012. Iris segmentation: State of the art and innovative methods, in: Liu, C., Mago, V. (Eds.), Cross Disciplinary Biometric Systems, Springer Berlin Heidelberg. pp. 151–182.

Donida Labati, R., Piuri, V., Ross, A., Scotti, F., 2019. DB QFIRE. http://homes.di.unimi.it/donida/dbqfire.php.

Donida Labati, R., Piuri, V., Scotti, F., 2009a. Agent-based image iris segmentation and multiple views boundary refining, in: Proc. 3rd IEEE Int. Conf. Biometrics: Theory, Appl. and Syst., pp. 204–210.

Donida Labati, R., Piuri, V., Scotti, F., 2009b. Neural-based iterative approach for iris detection in iris recognition systems. Proc. IEEE Symp. Computational Intell. Security and Defense Appl. , 1–6.

Donida Labati, R., Scotti, F., 2010. Noisy iris segmentation with boundary regularization and reflections removal. Image Vision Computing 28, 270–277.

Du, Y., Arslanturk, E., Zhou, Z., Belcher, C., 2011. Video-based noncooperative iris image segmentation. IEEE Trans. Syst., Man, Cybern. B, Cybern. 41, 64–74.

Feng, X., Fang, C., Ding, X., Wu, Y., 2006. Iris localization with dual coarse-

to-fine strategy, in: Proc. 18th Int. Conf. Pattern Recognition, pp. 553–556.
Gangwar, A., Joshi, A., 2016. Deepirisnet: Deep iris representation with applications in iris recognition and cross-sensor iris recognition, in: 2016 IEEE Int. Conf. on Image Processing, pp. 2301–2305.
Gangwar, A., Joshi, A., Singh, A., Alonso-Fernandez, F., Bigun, J., 2016. Irisseg: A fast and robust iris segmentation framework for non-ideal iris images, in: 2016 International Conference on Biometrics (ICB), pp. 1–8.
Gonzalez, R.C., Woods, R.E., 2006. Digital Image Processing. 3 ed., Prentice-Hall, Inc., Upper Saddle River, NJ, USA.
He, Y., Wang, S., Pei, K., Liu, M., Lai, J., 2017. Visible spectral iris segmentation via deep convolutional network, in: Chinese Conf. on Biometric Recognition, pp. 428–435.
He, Z., Sun, Z., Tan, T., Qiu, X., 2008a. Enhanced usability of iris recognition via efficient user interface and iris image restoration, in: Proc. 15th IEEE Int. Conf. Image Process., pp. 261–264.
He, Z., Tan, T., Sun, Z., Qiu, X., 2008b. Robust eyelid, eyelash and shadow localization for iris recognition, in: Proc. 15th IEEE Int. Conf. Image Process., pp. 265–268.
He, Z., Tan, T., Sun, Z., Qiu, X., 2009. Toward accurate and fast iris segmentation for iris biometrics. IEEE Trans. Pattern Anal. Mach. Intell. 31, 1670–1684.
Hofbauer, H., Alonso-Fernandez, F., Wild, P., Bigun, J., Uhl, A., 2014. A ground truth for iris segmentation, in: 2014 22nd Int. Conf. on Pattern Recognition, pp. 527–532.
Hollingsworth, K., Bowyer, K.W., Flynn, P.J., 2009. Pupil dilation degrades iris biometric performance. Compu. Vision and Image Understanding 113, 150–157.
Jain, A.K., Flynn, P., Ross, A.A., 2007. Handbook of Biometrics. Springer Sci. & Bus. Media, New York, NY, USA.
Jalilian, E., Uhl, A., 2017. Iris segmentation using fully convolutional encoder–decoder networks, in: Deep Learning for Biometrics, Springer International Publishing, Cham. pp. 133–155.
Jalilian, E., Uhl, A., Kwitt, R., 2017. Domain adaptation for cnn based iris segmentation, in: 2017 Int. Conf. of the Biometrics Special Interest Group (BIOSIG), pp. 1–6.
Jillela, R., Ross, A.A., 2013. Methods for iris segmentation, in: Burge, J.M., Bowyer, W.K. (Eds.), Handbook of Iris Recognition, Springer. pp. 239–279.
Jillela, R., Ross, A.A., Boddeti, V.N., Kumar, B.V.K.V., Hu, X., Plemmons, R., Pauca, P., 2013. Iris segmentation for challenging periocular images, in: Burge, J.M., Bowyer, W.K. (Eds.), Handbook of Iris Recognition, Springer, London, UK. pp. 281–308.
Jillela, R.R., Ross, A., 2014. Segmenting iris images in the visible spectrum with applications in mobile biometrics. Pattern Recognition Lett. .
Jobson, D., Rahman, Z.u., Woodell, G., 1997. A multiscale retinex for bridging the gap between color images and the human observation of scenes. IEEE Trans. Image Process. 6, 965–976.
Jobson, D., Rahman, Z.u., Woodell, G., 1997. Properties and performance of a center/surround retinex. IEEE Trans. Image Process. 6, 451–462.
Johnson, P., Lopez-Meyer, P., Sazonova, N., Hua, F., Schuckers, S., 2010. Quality in face and iris research ensemble (Q-FIRE), in: Proc. 4th IEEE Int. Conf. Biometrics: Theory, Appl. and Syst., pp. 1–6.
Kang, B., Park, K., 2005. A study on iris image restoration, in: Kanade, T., Jain, A., Ratha, N. (Eds.), Audio and Video-Based Biometric Person Authentication. Springer Berlin Heidelberg. volume 3546 of *Lecture Notes in Computer Science*, pp. 31–40.
Kang, B.J., Park, K.R., 2007. Real-time image restoration for iris recognition systems. IEEE Trans. Syst., Man, Cybern., B, Cybern. 37, 1555–1566.
Kennell, L.R., Rakvic, R.N., Broussard, R.P., 2009. Segmentation of off-axis iris images, in: Li, S.Z., Jain, A. (Eds.), Encyclopedia of Biometrics, Springer US, Boston, MA, USA. pp. 1158–1163.
Ko, J.G., Gil, Y.H., Yoo, J.H., Chung, K.I., . A novel and efficient feature extraction method for iris recognition. ETRI Journal 29, 399–401.
Kumar, A., Passi, A., 2010. Comparison and combination of iris matchers for reliable personal authentication. Pattern Recognition 43, 1016–1026.
Land, E.H., 1977. The retinex theory of color vision. Scientific Amer. 237, 108–128.
Li, P., Liu, X., Xiao, L., Song, Q., 2010. Robust and accurate iris segmentation in very noisy iris images. Image and Vision Computing 28, 246–253.
Li, Y.H., Savvides, M., 2013. An automatic iris occlusion estimation method based on high-dimensional density estimation. IEEE Trans. Pattern Anal. Mach. Intell. 35, 784–796.
Liu, N., Li, H., Zhang, M., Liu, J., Sun, Z., Tan, T., 2016. Accurate iris segmentation in non-cooperative environments using fully convolutional networks, in: 2016 Int. Conf. on Biometrics (ICB), pp. 1–8.
Liu, X., Li, P., Song, Q., 2009. Eyelid localization in iris images captured in less constrained environment, in: Proc. of the Third Int. Conf. on Biometrics, pp. 1140–1149.
Ma, L., Tan, T., Wang, Y., Zhang, D., 2004. Efficient iris recognition by characterizing key local variations. IEEE Trans. on Image Processing 13, 739–750.
Maio, D., Maltoni, D., Cappelli, R., Wayman, J., Jain, A., 2002. FVC2000: Fingerprint verification competition. IEEE Trans. Pattern Anal. Mach. Intell. 24, 402–412.
Makwana, R.M., 2010. Illumination invariant face recognition: A survey of passive methods. Procedia Comput. Sci. 2, 101–110.
Marsico, M.D., Galdi, C., Nappi, M., Riccio, D., 2014. Firme: Face and iris recognition for mobile engagement. Image and Vision Computing 32, 1161–1172.
Masek, L., Kovesi, P., 2003. MATLAB source code for a biometric identification system based on iris patterns.
Morley, D., Foroosh, H., 2017. Improving ransac-based segmentation through cnn encapsulation, in: IEEE Conf. on Computer Vision and Pattern Recognition (CVPR), pp. 2661–2670.
NEUROtechnology, . VeriEye. http://www.neurotechnology.com/verieye.html.
Nguyen, K., Fookes, C., Sridharan, S., Denman, S., 2010. Focus-score weighted super-resolution for uncooperative iris recognition at a distance and on the move, in: Proc. 25th Int. Conf. Image and Vision Computing New Zealand, pp. 1–8.
Nguyen, K., Fookes, C., Sridharan, S., Denman, S., 2011. Quality-driven super-resolution for less constrained iris recognition at a distance and on the move. IEEE Trans. Inf. Forensics Security 6, 1248–1258.
Nguyen, K., Sridharan, S., Denman, S., Fookes, C., 2012. Feature-domain super-resolution framework for Gabor-based face and iris recognition, in: Proc. IEEE Conf. Comput. Vision and Pattern Recognition, pp. 2642–2649.
Paris, S., Kornprobst, P., Tumblin, J., Durand, F., 2009. Bilateral Filtering: Theory and Applications. volume 4 of *Foundations and Trends in Computer Graphics and Vision*. Now Publishers Inc.
Parkhi, O.M., Vedaldi, A., Zisserman, A., 2015. Deep face recognition, in: British Machine Vision Conference, pp. 41.1–41.12.
Phillips, P.J., Scruggs, W.T., O'Toole, A.J., Flynn, P.J., Bowyer, K.W., Schott, C.L., Sharpe, M., 2010. Frvt 2006 and ice 2006 large-scale experimental results. IEEE Trans. on Pattern Analysis and Machine Intelligence 32, 831–846.
Proenca, H., Alexandre, L., 2012a. Toward covert iris biometric recognition: Experimental results from the NICE contests. IEEE Trans. Inf. Forensics Security 7, 798–808.
Proenca, H., Alexandre, L.A., 2007. The nice.i: Noisy iris challenge evaluation - part i, in: 2007 first IEEE Int. Conf. on Biometrics: Theory, Applications, and Systems, pp. 1–4.
Proenca, H., Alexandre, L.A., 2012b. Introduction to the special issue on the recognition of visible wavelength iris images captured at-a-distance and on-the-move. Pattern Recognition Lett. 33, 963–964.
Proenca, H., Filipe, S., Santos, R., Oliveira, J., Alexandre, L.A., 2010. The ubiris.v2: A database of visible wavelength iris images captured on-the-move and at-a-distance. IEEE Transactions on Pattern Analysis and Machine Intelligence 32, 1529–1535.
Proenca, H., Neves, J.C., 2017. Irina: Iris recognition (even) in inacurately segmented data, in: Proc. of the IEEE Conf. on Computer Vision and Pattern Recognition, CVPR 2017, pp. 1–10.
Proença, H., 2010. Iris recognition: On the segmentation of degraded images acquired in the visible wavelength. IEEE Trans. Pattern Anal. Mach. Intell. 32, 1502–1516.
Proença, H., Alexandre, L., 2006. Iris segmentation methodology for non-cooperative recognition. IEE Proc. Vision, Image and Signal Process. 153, 199–205.
Pundlik, S., Woodard, D., Birchfield, S., 2008. Non-ideal iris segmentation using graph cuts, in: Proc. IEEE Conf. Comput. Vision and Pattern Recognition Workshops, pp. 1–6.
Raja, K.B., Raghavendra, R., Vemuri, V.K., Busch, C., 2015. Smartphone based visible iris recognition using deep sparse filtering. Pattern Recogn. Lett. 57, 33–42.
Rathgeb, C., Uhl, A., 2010. Secure iris recognition based on local intensity variations, in: Campilho, A., Kamel, M. (Eds.), Image Analysis and Recognition, Springer Berlin Heidelberg, Berlin, Heidelberg. pp. 266–275.
Rathgeb, C., Uhl, A., Wild, P., 2013. Iris Recognition: From Segmentation to

Template Security. Springer, Berlin.
Rathgeb, C., Uhl, A., Wild, P., Hofbauer, H., 2016. Design decisions for an iris recognition sdk, in: Bowyer, K.W., Burge, M.J. (Eds.), Handbook of Iris Recognition, Springer London. pp. 359–396.
Ross, A., Shah, S., 2006. Segmenting non-ideal irises using geodesic active contours, in: Proc. Biometrics Symp. Special Session Res. Biometric Consortium Conf., pp. 1–6.
Roy, K., Bhattacharya, P., Suen, C.Y., 2010. Unideal iris segmentation using region-based active contour model, in: Campilho, A., Kamel, M. (Eds.), Image Analysis and Recognition, Springer Berlin Heidelberg. pp. 256–265.
Ryan, W., Woodard, D., Duchowski, A., Birchfield, S., 2008. Adapting starburst for elliptical iris segmentation, in: IEEE Int. Conf. Biometrics: Theory, Appl. and Syst., pp. 1–7.
Schmid, N.A., Zuo, J., Nicolo, F., Wechsler, H., 2013. Iris quality metrics for adaptive authentication, in: Burge, J.M., Bowyer, W.K. (Eds.), Handbook of Iris Recognition, Springer, London. pp. 67–84.
Scotti, F., Piuri, V., 2010. Adaptive reflection detection and location in iris biometric images by using computational intelligence techniques. IEEE Trans. Instrum. Meas 59, 1825–1833.
Shah, S., Ross, A., 2009. Iris segmentation using geodesic active contours. IEEE Trans. Inf. Forensics Security 4, 824–836.
Shamsi, M., Kenari, A., 2012. Iris boundary detection using an ellipse integro differential method, in: Proc. 2nd Int. Conf. Comput. and Knowledge Eng., pp. 1–5.
Shashua, A., Riklin-Raviv, T., 2001. The quotient image: Class-based rerendering and recognition with varying illuminations. IEEE Trans. Pattern Anal. Mach. Intell. 23, 129–139.
Shukri, D.S.M., Asmuni, H., Othman, R.M., Hassan, R., 2013. An improved multiscale retinex algorithm for motion-blurred iris images to minimize the intra-individual variations. Pattern Recognition Lett. 34, 1071–1077.
Simonyan, K., Zisserman, A., 2014. Very deep convolutional networks for large-scale image recognition. CoRR .
Sinha, N., Joshi, A., Gangwar, A., Bhise, A., Saquib, Z., 2017. Iris segmentation using deep neural networks, in: Int. Conf. for Convergence in Technology, pp. 548–555.
Sun, Z., Tan, T., 2009. Ordinal measures for iris recognition. IEEE Trans. on Pattern Analysis and Machine Intelligence 31, 2211–2226.
Tabassi, E., Grother, P., Salamon, W., 2011. Iris Quality Calibration and Evaluation (IQCE): Performance of Iris Image Quality Assessement and Algorithms. Technical Report. Nat. Inst. Standards and Technol. (NIST).
Tan, C.W., Kumar, A., 2012. Unified framework for automated iris segmentation using distantly acquired face images. IEEE Transactions on Image Processing 21, 4068–4079.
Tan, C.W., Kumar, A., 2013. Towards online iris and periocular recognition under relaxed imaging constraints. IEEE Trans. Image Process. 22, 3751–3765.
Tan, T., He, Z., Sun, Z., 2010. Efficient and robust segmentation of noisy iris images for non-cooperative iris recognition. Image Vision Computing 28, 223–230.
Tan, X., Triggs, B., 2010. Enhanced local texture feature sets for face recognition under difficult lighting conditions. IEEE Trans.on Image Processing 19, 1635–1650.
The Center of Biometrics and Security Research, . CASIA-IrisV4. http://biometrics.idealtest.org.
Thornton, J., Savvides, M., Kumar, B.V.K.V., 2007. A bayesian approach to deformed pattern matching of iris images. IEEE Trans. on Pattern Analysis and Machine Int. 29, 596–606.
Tomeo-Reyes, I., Ross, A., Clark, A.D., Chandran, V., 2015. A biomechanical approach to iris normalization, in: Proc. Int. Conf. on Biometrics, pp. 9–16.
Wang, H., Li, S., Wang, Y., 2004. Generalized quotient image, in: Proc. IEEE Conf. Comput. Vision and Pattern Recognition, pp. 498–505.
Wang, K., Qian, Y., 2011. Fast and accurate iris segmentation based on linear basis function and RANSAC, in: Proc. 18th IEEE Int. Conf. Image Process., pp. 3205–3208.
Wild, P., Hofbauer, H., Ferryman, J., Uhl, A., 2015. Segmentation-level fusion for iris recognition, in: Proc. of the 2015 Int. Conf. of the Biometrics Special Interest Group, pp. 1–6.
Wildes, R.P., 1997. Iris recognition: An emerging biometric technology. Proc. IEEE 85, 1348–1363.
Yang, G., Zeng, H., Li, P., Zhang, L., 2015. High-order information for robust iris recognition under less controlled conditions, in: 2015 IEEE Int. Conf. on Image Processing (ICIP), pp. 4535–4539.
Yang, T., Stahl, J., Schuckers, S., Hua, F., Boehnen, C.B., Karakaya, M., 2014. Gaze angle estimate and correction in iris recognition, in: Proc. IEEE Symp. Computational Intelligence in Biometrics and Identity Management, pp. 132–138.
Zhang, X., Sun, Z., Tan, T., 2010. Texture removal for adaptive level set based iris segmentation, in: Proc. 17th IEEE Int. Conf. Image Process., pp. 1729–1732.
Zhao, Z., Kumar, A., 2015. An accurate iris segmentation framework under relaxed imaging constraints using total variation model, in: 2015 IEEE Int. Conf. on Computer Vision (ICCV), pp. 3828–3836.
Zhao, Z., Kumar, A., 2017. Towards more accurate iris recognition using deeply learned spatially corresponding features, in: IEEE Int. Conf. on Computer Vision, pp. 3829–3838.
Zuo, J., Kalka, N., Schmid, N., 2006. A robust iris segmentation procedure for unconstrained subject presentation, in: 2006 Biometrics Symp. Special Session Res. Biometric Consortium Conf., pp. 1–6.
Zuo, J., Schmid, N., 2010. On a methodology for robust segmentation of nonideal iris images. IEEE Trans. Syst., Man, Cybern., B, Cybern. 40, 703–718.